J. Fluid Mech. (1981), *vol.* 108, *pp.* 195–226
Printed in Great Britain

Steady-state two-dimensional detonation

By J. B. BDZIL

University of California, Los Alamos Scientific Laboratory,
Los Alamos, New Mexico 87545

(Received 20 December 1979 and in revised form 24 October 1980)

An analytical steady-state theory of the detonation 'diameter effect' is presented. This theory, which includes the off-axis flow, is a generalization of the Wood–Kirkwood analysis. When the state dependence of the reaction rate is stronger than that of the product of the sound speed squared and the flow divergence, detonation failure can occur. The leading term in the extrapolation of the detonation velocity to infinite charge size is quadratic in the inverse charge size and not linear as popularly believed. When calibrated to the detonation velocity *vs.* charge-size data, the theory reproduces the limited amount of experimental shock loci to a high degree of accuracy.

1. Introduction

It is experimentally known that a detonation wave in a high-density explosive propagating along the axis of a right-circular cylinder (rate stick) reaches a steady-state velocity that is a function of both the cylinder radius and the properties of the inert material confining the explosive cylinder. As the radius of the explosive cylinder, r^*, is decreased the detonation velocity decreases until the radius reaches a critical value, r_f, below which no steady-state detonation is observed. This phenomenon, which is called the detonation diameter effect, was recently reviewed (Campbell & Engelke 1976). They showed that, for twelve heterogeneous high-density solid explosives,† confined by ambient air, and for two liquid explosives, one confined in brass, the other in glass, the data could be fitted to the relation

$$l \equiv D/D_{cj} = 1 - A/(r^* - r_c). \tag{1.1}$$

where D is the detonation velocity at radius r, D_{cj} is the one-dimensional steady-state (Chapman–Jouguet) detonation velocity, and A and r_c are fitting parameters. For most of the solid explosives they examined

$$r_c = 0{\cdot}88 r_f, \tag{1.2}$$

so that the diameter effect (l *vs.* r^{*-1}) is downward concave. Near failure, the slope is steep and $l = O(0{\cdot}9)$. For the liquid explosives, the diameter effect is linear ($r_c \simeq 0$) and $l = O(0{\cdot}99)$ at failure. The notable exceptions to equation (1.2) were the TATB (triamino-trinitrobenzene) formulations at about 98 % of theoretical maximum density. The TATB formulations had zero or slightly negative values of r_c so that (1.1) gives a linear diameter effect for them, similar to that observed for liquid explosives. Since liquid explosives are throught to fail because of a failure-wave-type instability,

† These include HMX, RDX, TNT and TATB based explosives and HMX/TNT and RDX/TNT mixtures.

Campbell & Engelke postulated that the failure mechanism is different for explosives with a downward concave diameter effect from those with a linear diameter effect. We speculate that a downward concave diameter effect is obtained when it is no longer possible to construct a two-dimensional steady-state solution, as discussed by Tsugé *et al.* (1970); a linear diameter effect is obtained when a two-dimensional steady-state solution is unstable to small fluctuations for $l = O(0{\cdot}99)$. Clearly, detonation in a rate stick composed of a heterogeneous explosive can strictly be neither two-dimensional nor steady-state. However, experimentally, it is known that, after an initial transient phase, the detonation velocity is relatively constant and that the shock shape is symmetrical and reproducible. Therefore, as a first approximation to the real behaviour, we might assume that the process is steady-state and two-dimensional. Considering that such a large number of diameter effect curves are similar (downward concave) and that far from failure even detonations in liquid explosives probably propagate via a quasi steady-state mode, it would be useful to have a theory for steady-state two-dimensional detonation in high-density explosives. When appropriately calibrated, such a theory could provide some information about the heat release processes that support the detonation.

A number of theoretical studies of this phenomenon have been made. Common to all of these is the assumption that the streamlines diverge from the head-on direction, and as a consequence act as a mass sink in the one-dimensional continuity equation. Jones (1947) developed an approximate nozzle theory for the problem and related the area divergence to the charge size. Eyring *et al.* (1949) based their theory on the observation that the shock is curved for most solid high explosives. Using the continuity of mass for a spherical system, they derived a relation between the detonation velocity and shock curvature. Using this relation, they did a graphical construction for the shock in a cylindrical rate stick. For an uncased charge, this gives them

$$l = 1 - 0{\cdot}5z^*/r^*, \tag{1.3}$$

where z^* is the one-dimensional reaction-zone length. Both of these theories are, at best, only semi-quantitative. However, they define the two fundamental models that all subsequent work has followed.

Wood & Kirkwood (1954) took the assumption of a curved shock front, introduced by Eyring, and added the assumption that the radius of curvature of the shock was large compared with the reaction-zone length. Expanding the solution in a formal power series in $(z^*/\hat{S})$, they showed that to $O(z^*/\hat{S})$ (i.e. all terms up to and including order one in the expansion are retained)

$$l \sim 1 - \beta z^*/\hat{S}, \tag{1.4}$$

where $\hat{S}$ is the central radius of curvature of the shock, and β is an available constant. Unlike the previous work, equation (1.4) is rigorous.

More recently, Tsugé *et al.* (1970) applied the nozzle theory to gaseous detonation, where the assumption of a flat shock is a reasonable one. Studying the detonation of H_2/O_2 confined by an inert gas, they calculated the channel area in the nozzle in the limit that the confining inert could be treated with the Newton hypersonic approximation (Hayes & Probstein 1966). They then calculated the diameter effect for H_2/O_2, including the detonation-failure state and a second low-velocity detonation mode.

The purpose of this paper is to present a relatively complete description of the diameter effect for high-density explosives. Since detonation in these materials is

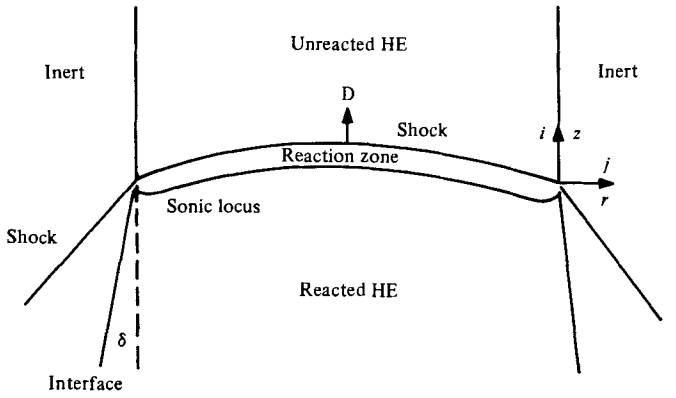

FIGURE 1. A schematic representation of a two-dimensional steady-state detonation in a high-density explosive.

characterized by curved shocks, nozzle theories are automatically excluded. What we will do is show how the Wood–Kirkwood theory can be extended so as to permit one to calculate the diameter effect, the shock locus, and the detonation-failure state.

In § 2, we present the governing differential equations and boundary conditions. We develop the generalized Wood–Kirkwood approximation to the radial flow and use it to get the basic governing equation for the problem [equation (3.14)], in § 3. In § 4, we solve equation (3.14) in conjunction with a special heat release law to get a simple model of steady-state two-dimensional detonation [equation (4.8)]. We discuss the features of the model, including the form of the diameter effect [equation (5.8)] and shock locus [equation (5.11)], in § 5. In § 6, we show that the model is in good agreement with experimental data on two-dimensional detonation.

2. Steady-state flow equations

Figure 1 shows a schematic representation of the flow problem we wish to consider. A two-dimensional detonation, consisting of a reaction zone preceded by a curved shock, propagates into a quiescent explosive. The chemical reaction, which is initiated by the shock, goes to completion at or beneath the locus of sonic flow. The pressure generated by the reaction deflects the confining inert, thereby causing the streamlines in the explosive to deflect by an amount $\delta \equiv |u_{r+}/u_{z+}|$ at the intersection of the shock with the confining inert. We assume that the entire process is steady in the reference frame of the detonation shock, and that the Euler equations provide an adequate description of the mechanics.

For convenience, we assume that our co-ordinate system is attached to the shock which travels with velocity $D\mathbf{i}$. With these assumptions, the material derivative is $d/dt = \hat{\mathbf{u}}.\nabla - D\,\partial/\partial z$ so that the Euler equations become

$$\nabla.(\rho\mathbf{u}) = 0, \tag{2.1}$$

$$\mathbf{u}.\nabla\mathbf{u} + \frac{1}{\rho}\nabla P = 0, \tag{2.2}$$

$$\mathbf{u}.\nabla E - \frac{P}{\rho^2}\mathbf{u}.\nabla\rho = 0, \tag{2.3}$$

where the independent variables are (z, r) and the dependent variables ρ, $\mathbf{u}$, $(\hat{\mathbf{u}})$, P, E, are the density, shock (laboratory) centred particle velocity, pressure, and specific internal energy, respectively. If we assume that the detonation is driven by a single chemical reaction (or a set of reactions which combine to give one effective forward exothermic heat release) and that the equation of state of the reactants and products is the same, then

$$E = e(P, \rho) - q\lambda, \tag{2.4}$$

where q is the heat of detonation, and λ is the reaction progress variable,

$$0 \leqslant \lambda \leqslant 1,$$

with $\lambda = 0$ corresponding to unreacted material and where $\lambda = 1$ marks the end of the reaction zone.

We begin by rewriting (2.1) in a form more suitable for analysis. Substituting (2.4) into (2.3) and then eliminating $\mathbf{u} \cdot \nabla P$ with (2.2), gives

$$\tfrac{1}{2}\rho \mathbf{u} \cdot \nabla u^2 + c^2 \mathbf{u} \cdot \nabla \rho = -qR/(\partial e/\partial P),$$

where R is the steady-state reaction rate

$$\mathbf{u} \cdot \nabla \lambda = R.$$

Using this equation to eliminate $\mathbf{u} \cdot \nabla \rho$ in (2.1) produces (2.1) in the desired form

$$(c^2 - u_z^2)\frac{\partial u_z}{\partial z} - 2u_z u_r \frac{\partial u_r}{\partial z} + (c^2 - u_r^2)\frac{\partial u_r}{\partial r} + \alpha c^2 \frac{u_r}{r} = qR \Big/ \left[\rho\left(\frac{\partial e}{\partial P}\right)\right] - u_z u_r \Omega, \tag{2.5}$$

where α equals zero (one) corresponds to plane (cylindrical) symmetry, c is the sound speed at fixed λ, and Ω is the vorticity of the flow

$$\Omega = \frac{\partial u_r}{\partial z} - \frac{\partial u_z}{\partial r}. \tag{2.6}$$

Equation (2.5) is a particularly convenient form for calculations since it explicitly displays how the two-dimensional effects modify the one-dimensional equation. In the absence of any two-dimensionality, only the first terms of both the right- and left-hand side of equation (2.5) appear. They correspond, respectively, to the rate of chemical energy addition and the longitudinal propagation of acoustic energy and convection of kinetic energy. When the flow is two-dimensional, the longitudinal transport of energy is modified to include the convection of the added radial kinetic energy

$$-u_z u_r \frac{\partial u_r}{\partial z},$$

and energy is diverted from longitudinal transport to radial transport by

$$c^2 \frac{\partial u_r}{\partial r} - \tfrac{1}{2} u_r \frac{\partial}{\partial r}(u_z^2 + u_r^2) + \alpha c^2 \frac{u_r}{r},$$

where we have made use of the identity

$$u_z u_r \Omega - 2u_z u_r \frac{\partial u_r}{\partial z} = -u_z u_r \left(\frac{\partial u_r}{\partial z} + \frac{\partial u_z}{\partial r}\right).$$

For the systems we wish to consider, the state ahead of the shock is homenergic. Equation (2.3) then reduces to the strong form of Bernoulli's law, which in the strong-shock approximation is

$$e(P,\rho)+P/\rho+\tfrac{1}{2}|\mathbf{u}|^2-q\lambda=\tfrac{1}{2}D^2, \tag{2.7}$$

where D is the detonation velocity.

To complete the specification of the problem we need to specify the constitutive relations and the boundary conditions. As constitutive relations, we take a polytropic equation of state

$$e=\frac{1}{\gamma-1}\frac{P}{\rho}, \tag{2.8}$$

where γ is the polytropic exponent, and a state-dependent rate law

$$R=k(c^2/c_{cj}^2)\,g(c^2/c_{cj}^2, P/P_{cj}, \ldots, \lambda), \tag{2.9}$$

where k is the rate multiplier and g is as yet an arbitrary function. The form of (2.9) was selected for the convenience of the calculations in §4. The boundary conditions must be applied along three distinct curves; the piston surface (rear boundary of the explosive), the interface separating the explosive from the confining inert, and the detonation shock. In this paper, we will restrict our attention to studying the reaction-zone structure. Assuming that the piston velocity is sufficiently low, the piston condition decouples from the reaction-zone structure. Second, we assume that the interface separating the explosive from the inert is a slip-line free boundary along which the pressure and streamline deflection are continuous. Finally, along the free-boundary shock locus we have the conditions (Hayes & Probstein 1966)

$$\frac{\rho_0}{\rho_+}=\frac{\gamma-1}{\gamma+1}, \tag{2.10}$$

$$u_{z+}=-D\left[\frac{\gamma-1}{\gamma+1}+\left(\frac{dz_s}{dr}\right)^2\right]\left[1+\left(\frac{dz_s}{dr}\right)^2\right]^{-1}, \tag{2.11}$$

$$u_{r+}=-\frac{2}{\gamma+1}D\frac{dz_s}{dr}\left[1+\left(\frac{dz_s}{dr}\right)^2\right]^{-1}, \tag{2.12}$$

and

$$P_+=\frac{2\rho_0 D^2}{\gamma+1}\left[1+\left(\frac{dz_s}{dr}\right)^2\right]^{-1}, \tag{2.13}$$

where $z_s(r)$ is the shock locus and the $+$ subscript denotes the shock value. In the next section we derive the generalized Wood–Kirkwood approximation.

3. The generalized Wood–Kirkwood theory

The central approximations in the Wood–Kirkwood theory of the diameter effect (Wood & Kirkwood 1954) are the result of the following assumptions: (1) the explosive charge size is large compared with the one-dimensional reaction-zone length and (2) the radius of curvature of the shock is large compared with the one-dimensional reaction-zone length. Figure 2 shows a schematic representation of the Wood–Kirkwood reaction zone. Even though Wood–Kirkwood introduced these concepts and applied them in their theory, they did not fully utilize all of the implications. What

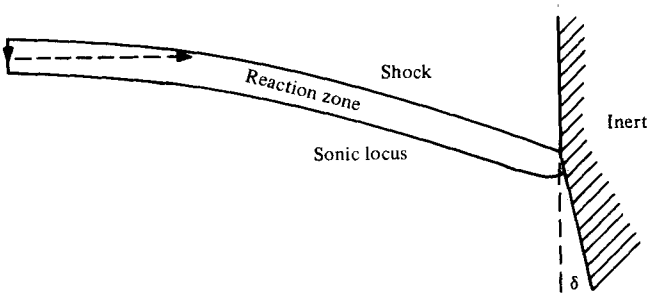

FIGURE 2. A schematic representation of the Wood–Kirkwood two-dimensional reaction zone.

we will do is show how the entire flow can be calculated when, in addition to the Wood–Kirkwood approximations, we assume that the streamline deflection angle remains small.

The assumptions of Wood–Kirkwood can be translated into precise mathematical expressions. In appendix A, we show that the contribution of the vorticity to the energetics of the flow is small compared with the contribution of the chemical reaction. Using this result, we derive an equation for the streamline deflection angle in appendix B, equation (B 19),

$$\frac{\partial}{\partial z}(u_r/u_z) = \frac{u_2 qR[1+(z_s')^2]^{-\frac{1}{2}}}{u_z^2(u_1^2-c^2)\rho\left(\dfrac{\partial e}{\partial P}\right)} + O[(u_r/u_z)S^{-1}], \tag{3.1}$$

where

$$u_1 = (u_z - z_s' u_r)[1+(z_s')^2]^{-\frac{1}{2}}, \tag{3.2}$$

$$u_2 = (z_s' u_z + u_r)[1+(z_s')^2]^{-\frac{1}{2}}, \tag{3.3}$$

and

$$S^{-1} = -z_s''[1+(z_s')^2]^{-\frac{3}{2}}, \tag{3.4}$$

where S is the radius of curvature of the shock. Equation (3.1) states that the reactivity curves the streamlines toward the axis of symmetry in the subsonic part of the flow (most of the reaction zone). This is simply a consequence of the assumption that the detonation shock is not strongly curved so that the pressure gradient through the reaction zone is large compared with the pressure gradient along the shock. Equation (3.1) is both a new and an interesting result. It states that, in reactive flows for which the vorticity can be neglected, the streamline curvature is related to both the sign of the energy release and the sonic character of the flow.

Next, we consider the magnitude of the streamline deflection angle. The tangent of the deflection angle at the shock can be obtained from equations (2.11) and (2.12):

$$\delta = -\frac{2}{\gamma+1} z_s' \left[\frac{\gamma-1}{\gamma+1} + (z_s')^2\right]^{-1}. \tag{3.5}$$

In appendix C we show that at the charge boundary the flow in the shock fixed reference frame must be either subsonic for a heavily confined charge or sonic for an unconfined charge. If we neglect the vorticity, it then follows that

$$(z_s')^2 \leqslant \frac{\gamma-1}{\gamma+1}, \tag{3.6}$$

and

$$\delta \leqslant (\gamma^2-1)^{-\frac{1}{2}}. \tag{3.7}$$

For most solid high-explosives γ is near 3·0. Therefore, in view of the results contained in (3.1) and (3.7), the tangent of the streamline deflection angle will be less than about one-third. This is small enough to justify the assumption that the streamline deflection angle remains small. We will assume that $z_s' = O(\delta)$. Nevertheless, (3.14) yields solutions with the correct asympotic dependence for $z_s' = O(1)$.

One comment is in order concerning the validity of neglecting the vorticity. Near the charge boundary, the deflection of the streamlines in the high-explosive must match that of the streamlines in the confining inert. Since there is a discontinuity in the reactivity as we pass from the high-explosive into the confining inert, the analogue of (3.1) for the inert leads us to the conclusion that the streamlines in the inert are more nearly straight lines. In turn, it follows that the vorticity must be important in the high-explosive near the inert boundary. It can be shown that this boundary region extends into the explosive for approximately one reaction-zone length (see appendix F).

Taking advantage of the smallness of the deflection angle, we can find a first approximation to the solution of (3.1). Replacing $qR[u_z(u_1^2 - c^2)\rho(\partial e/\partial P)]^{-1}$ by its one-dimensional value $-d(\ln u_z)/dz$ in (3.1) gives us an equation which readily integrates to

$$u_r = -z_s'[u_z + D(u_z/u_{z+})^{a(z_s')}] + O(\delta^3) + O(\delta S^{-1}), \tag{3.8}$$

where

$$a(z_s') = (z_s')^2/[1 + (z_s')^2]. \tag{3.9}$$

For values of γ near 3·0, the factor $(u_z/u_{z+})^{a(z_s')}$ does not deviate from one by more than 10%. Therefore, we get as our approximation to the radial velocity

$$u_r = -z_s' \frac{D}{(\gamma+1)}(1+t) + O(\delta^3) + O(\delta S^{-1}), \tag{3.10}$$

$$t \equiv (1-\lambda)^{\frac{1}{2}}, \tag{3.11}$$

where we have replaced u_z by its one-dimensional value.

Equation (3.10) is a mathematical statement of our generalization of the Wood–Kirkwood theory of two-dimensional detonation. It states that u_r depends on r only through z_s' and decreases by a factor of two from the shock to the end of the reaction zone. We will use this result in equation (2.5) to calculate our two-dimensional detonation. Higher approximations to u_r can be found by treating the problem with singular perturbation theory with $(z, \delta r)$ as the independent variables and expanding the solution in a power series in δ (see appendix D). However, the purpose of this calculation is to display the properties of two-dimensional detonation as clearly as possible. Therefore, we will not include any higher approximations to u_r than are contained in (3.10). When higher approximations are included, only a small quantitative change occurs in the solution.

If we are to describe the reaction-zone structure shown in figure 2, it will be convenient to transform to independent variables that are locally fixed to the shock. We will transform to t, r as independent variables, where

$$\frac{\partial t}{\partial z} = -\frac{R}{2tu_z} - \frac{u_r}{u_z}\frac{\partial t}{\partial r}, \tag{3.12}$$

and

$$\frac{\partial t}{\partial r} = -z_s'\frac{\partial t}{\partial z} + O(\delta^3) + O(\delta S^{-1}). \tag{3.13}$$

With the use of (3.13), (3.12) and (3.10), we can now rewrite (2.5) as an ordinary differential equation for u_z with t as the independent variable and r as a parameter (see appendix E)

$$(\hat{c}^2 - u_z^2)\frac{du_z^2}{dt} + 4tu_z^2\hat{c}^2 D[R(\gamma+1)]^{-1}\left(z_s'' + \frac{\alpha}{r}z_s'\right)(1+t) + 2tu_z^2 D_{cj}^2(\gamma+1)^{-1}$$
$$= \tfrac{1}{2}D_{cj}^4(\gamma+1)^{-3}(z_s')^2 f(t) + O(\delta^4) + O(\delta^2 S^{-1}) + O(S^{-2}), \quad (3.14)$$

where $\hat{c}^2$ (the fixed composition sound speed on the central streamline) and $f(t)$ are given in appendix E. That is, equation (3.14) describes the evolution of u_z^2 along a streamline. For most solid high-explosives, the detonation velocity deficit at failure and correspondingly the scaled value of S^{-1} are $O(10^{-1})$ (Campbell & Engelke 1976). Therefore, the terms that we have neglected in deriving (3.14) represent no more than an $O(10^{-2})$ effect.

To help in understanding the physical nature of the solutions of (3.14) that appear in the next section, we briefly describe the physical nature of the terms in (3.14). The terms on the left-hand side are present everywhere in the flow including the symmetry plane (line). Along the central streamline ($z_s' = 0$), they reduce to the quasi-one-dimensional approximation. The explicit term on the right-hand side vanishes on the symmetry plane (line). Term by term, we have:

Left-hand side:

(1) the energy diverted to the longitudinal motion;
(2) the energy diverted to streamline divergence. This term is proportional to the ratio of the mean shock curvature to the reaction rate, where $-\frac{1}{2}(z_s'' + (\alpha/r)z_s')$ is an approximation to the mean shock curvature [$O(\delta^2)$ terms omitted];
(3) the chemical energy release.

Right-hand side:

(1) the energy diverted to the lateral motion, being proportional to the square of the streamline deflection angle;
(2) energy diverted to rotational motion, etc.

Therefore, we find that by generalizing the Wood–Kirkwood assumption concerning a two-dimensional reaction zone, we can reduce the partial differential equations describing the complete reaction zone to a set of ordinary differential equations, with t as the independent variable and r as a parameter. If the reaction rate depends only on the independent variable t and on the dependent variable c^2 (i.e. on u_z, u_r and t), then the set of ordinary differential equations reduces to equation (3.14). In the next section we present the solution to these equations for a model rate law.

4. A simple detonation model

In deriving equation (3.14), the radial flow has been approximated by (3.10). Therefore, the boundary condition along the high-explosive/inert boundary cannot be satisfied exactly, but only in an average sense (see appendix F). Since the initial integration of equation (3.14) treats t as the only independent variable, we will postpone considering the inert boundary until later. Two conditions remain that must be satisfied by the solution of (3.14); they are: (1) the conditions at the shock boundary, and (2) those at the singularity that occur when $(\hat{c}^2 - u_z^2) = 0$.

To facilitate the analysis, we introduce the change of variables

$$l \equiv \frac{D}{D_{cj}}, \quad \phi \equiv \frac{(\gamma+1)^2}{D_{cj}^2} u_z^2, \quad \epsilon \equiv -\frac{2\gamma^2}{(\gamma+1)^2} \frac{D_{cj}}{k} \left(z_s'' + \frac{\alpha}{r} z_s' \right) \tag{4.1a,b,c}$$

into (3.14), to get

$$[l^2(\gamma^2-1)+1-t^2-\phi] \frac{d\phi}{dt} + 4t\phi[1 - l\epsilon(1+t)\, g^{-1}] = (z_s')^2 f(t), \tag{4.2}$$

where g and k are defined in (2.9). Equation (4.2) is an ordinary differential equation in t for $\phi(t; r, l)$ with r appearing as a parameter in z_s' and ϵ. At the shock, equation (2.11) requires that

$$\phi(t=1) = l^2[(\gamma-1)^2 + 4(\gamma-1)\,(z_s')^2 + O(\delta^4)], \tag{4.3}$$

and at the singularity, which we define to be at t^*, (4.2) gives us the two equations

$$l^2(\gamma^2-1) + 1 - t^{*2} - \phi(t=t^*) = 0 \tag{4.4a}$$

and

$$4t^*\phi(t=t^*)\,[1 - l\epsilon(1+t^*)\, g(t=t^*)^{-1}] - (z_s')^2 f(t^*) = 0. \tag{4.4b}$$

When the solution of (4.2) is forced to satisfy (4.3) and (4.4), we get a differential relation involving l, ϵ, z_s' and r. This relation, together with some average streamline deflection condition at the explosive/inert boundary, gives us a differential condition from which we can obtain the diameter effect and the shock locus for an explosive in a given geometry with a given confinement.

Before we can proceed to solve (4.2) we must define a rate law. For the purposes of this demonstration, we will require that the rate have two properties. First, we would like the rate to depend on the thermodynamic state, say the pressure. Second, we will require simplicity in the form of the solution to (4.2), (4.3) and (4.4). The rate

$$\left.\begin{aligned} R &= k(c^2/c_{cj}^2)\, l^n (1+t)\, \phi, \quad 0 < t \leqslant 1, \\ R &= 0, \qquad\qquad\qquad\quad t = 0, \end{aligned}\right\} \tag{4.5}$$

where $t = (1-\lambda)^{\frac{1}{2}}$, includes both properties. The dependence on the local thermodynamic state via c^2 and on the shock state via l^n, gives us the desired state dependence. The somewhat unrealistic factor $(1+t)\,\phi$ gives us the desired simplicity. When equation (4.5) is substituted into (4.2), we get an Abel first-order differential equation of the second kind. Other, perhaps more 'realistic', rates could be used but in that case equation (4.2) would require numerical integration. For such cases, the analytic structure of the solution would be lost, thereby making the solution more difficult to interpret.

Treating the off-axis term in (4.2) as a perturbation, we can use Lighthill's stretched co-ordinate technique (Comstock 1972) to solve (4.2). Equation (4.2) is a singular perturbation problem, because (4.4a) must be satisfied (the flow must be sonic) at some point in $0 \leqslant t \leqslant 1$. Retaining only first-order terms in the perturbation, we find

$$\phi = 2\epsilon l^{1-n} - l^2(\gamma^2-1) - 1 + \eta^2 + H(r) \pm \{H^2(r) + 2H(r)\,[\epsilon l^{1-n} - l^2(\gamma^2-1) - 1 + \eta^2]\}^{\frac{1}{2}}, \tag{4.6}$$

where we have taken care that the stretched co-ordinate η,

$$\eta^2 = t^2 - t\left(t + \frac{2\gamma+1}{\gamma}\right)(z_s')^2 + O(\delta^4), \tag{4.7}$$

reduces to t at the critical point (sonic point). Here, $H(r)$ is an arbitrary function introduced by the integration. Because of our choice of the rate law, (4.6) is identical in form to the one-dimensional solution. As in that case, we choose the strong detonation branch (Fickett & Davis 1979). Requiring that equation (4.6) satisfy the shock and singularity conditions of (4.3) and (4.4), we find that we can have a solution to our problem if, and only if,

$$l^4 - l^2 + l^{1-n}\kappa - (z_s')^2 = 0, \tag{4.8}$$

where the scaled mean shock curvature κ is

$$\kappa \equiv (\gamma-1)^{-2}\epsilon = \frac{-2\gamma^2}{(\gamma^2-1)^2}\frac{D_{cj}}{k}\left(z_s'' + \frac{\alpha}{r}z_s'\right). \tag{4.9}$$

Equation (4.8) is our differential condition relating l, ϵ, z_s' and r. It can readily be integrated to get the shock locus and detonation velocity as a function of the charge size.

At this point in our calculation, the formal solution of the problem is complete. In the next section, we will examine some of the properties of the solution.

5. Discussion of the results

Equation (4.8) provides the basis for our discussion. We begin by first considering the central streamline limit of equation (4.8)

$$l^{3+n} - l^{1+n} + \hat{\kappa} = 0, \tag{5.1}$$

where $\hat{\kappa}$ is the scaled mean shock curvature on the central streamline. We note that $\hat{\kappa}$ contains the factor $(1+\alpha)$. Therefore, for a given detonation velocity deficit, twice the experimentally measured shock curvature is needed in charges of plane symmetry as in those of cylindrical symmetry.

Linearizing equation (5.1) in the velocity deficit, we get the Wood–Kirkwood result, (1.4). Retaining the nonlinearities in (5.1), we find that $l(\hat{\kappa})$ can be double-valued when $n > -1$. The two branches of the curve meet at the point where $(dl^2/d\hat{\kappa}) = \infty$;

$$l_f^2 = \frac{1+n}{3+n}, \tag{5.2a}$$

$$\hat{\kappa}_f = l_f^{1+n}\frac{2}{3+n}. \tag{5.2b}$$

Since no solutions can be found for $\hat{\kappa} > \hat{\kappa}_f$ when $n > -1$, we call equation (5.2) the detonation failure condition. Therefore, when the nonlinearities in the rate are retained, the model can show detonation failure. Of the two branches of $l(\hat{\kappa})$, we will consider only the upper branch, the so-called high-order detonation branch. For a discussion of the possible significance of the lower branch (see Tsugé *et al.* 1970; Zeldovich & Kompaneets 1960).

From equation (5.1), we find that at $l^2 = 1$ the slope $dl^2/d\hat{\kappa}$ is independent of n and depends only on the one-dimensional reaction-zone length. Also, for $n > -1$, l^2 *vs.* $\hat{\kappa}$ is downward concave with the curves of smaller n providing a bound from above for those of larger n. The slope of l *vs.* $\hat{\kappa}$ at the failure point defined by (5.2) is infinite, and

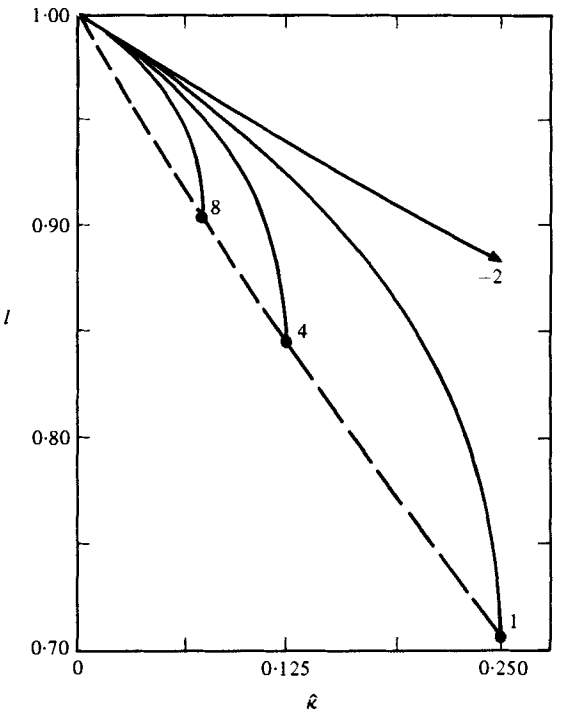

FIGURE 3. The detonation-velocity fraction (l) *vs.* the scaled central streamline mean shock curvature ($\hat{\kappa}$) for the rate law of (4.5), with $n = -2$, 1, 4 and 8. The dots indicate the point of detonation failure as defined by (l_f, $\hat{\kappa}_f$), and the dashed line is the failure locus. The $n = -2$ curve does not show failure.

as n is increased $\hat{\kappa}_f$ decreases and l_f^2 increases. Figure 3 shows l *vs.* $\hat{\kappa}$ for a number of different values of n.

The failure condition given by (5.2) is sufficient to ensure failure in the sense that no solutions are found for $\hat{\kappa} > \hat{\kappa}_f$. However, since (4.8) and not (5.1) is the constraint relating l^2, κ, z_s' and r, equation (5.2) may not be a necessary condition at failure. We define detonation failure as: the pair l, $r^*(l_f, r_f)$ for which (4.8) and the boundary condition at r^* no longer have a solution for r satisfying $0 \leqslant r \leqslant r^*$.

For a polytropic equation of state, (4.5) will lead to failure only when $n > -1$. This leads to the question: Why must the rate law exceed a critical state dependence before it exhibits failure? We can gain some insights into this question by examining the terms in (4.2) corresponding to the energy release rate and central streamline divergence. At the shock these terms are

$$4(\gamma-1)^2 l^2(1-\hat{\kappa} l^{-1-n}), \tag{5.3}$$

where the first term is the reactive source and the second term is the divergence loss. The important question seems to be: What qualitative change occurs in (5.3) as we change n? At failure

$$\hat{\kappa}_f l_f^{-1-n} = \frac{2}{3+n}, \tag{5.4}$$

so that (5.3) does not necessarily go through a zero at the failure point. What does change as we change n is the nature of the feedback that l has on the 'effective' flow divergence ($\hat{\kappa} l^{-1-n}$). For $n = -2$, equation (5.3) becomes

$$4(\gamma - 1)^2 l^2 (1 - \hat{\kappa} l), \tag{5.5}$$

so that, as $\hat{\kappa}$ is increased, which leads to a decrease in l, l moderates the increase in the effective flow divergence. This is a negative feedback. Whereas, for $n = 0$, equation (5.3) becomes

$$4(\gamma - 1)^2 l^2 (1 - \hat{\kappa} l^{-1}), \tag{5.6}$$

so that, as $\hat{\kappa}$ is increased, l accelerates the growth of the effective flow divergence. This is a positive feedback. Therefore, we speculate that failure occurs only for rates which generate positive feedback. For $n = -1$, the state dependence of the rate, (4.5), goes like l^3 and that of the divergence term [$c^2 \partial u_r/\partial r$ in (2.5)] also goes like l^3. Generalizing to an arbitrary rate, the existence of detonation failure requires that the state dependence of the energy release be greater than that of $c^2 \partial u_r/\partial r$. For the popular power-law pressure dependent rate law [equation (D 1)], we can show, using the type of analysis described in appendix D, that a linear burning (P) will not lead to failure, whereas a quadratic burning (P^2) will show failure.

Up to this point our discussion has been limited to only the central streamline. Equation (4.8) contains information about the off-axis flow as well. Adding information about the high-explosive streamline at the explosive/inert boundary, we can integrate equation (4.8) to get the shock locus. As was discussed in § 3 and appendix C, the details of the explosive/inert interaction are not treated properly by this analysis. Fortunately these details extend laterally into the flow no more than one reaction-zone length (see appendix F and Bdzil 1976), at which point the lateral boundary condition is

$$\delta \mathscr{L} = -\frac{2}{\gamma + 1} z_s'(r^*) \left[\frac{\gamma - 1}{\gamma + 1} + (z_s'(r^*))^2\right]^{-1}, \tag{5.7}$$

where δ is the streamline deflection angle at the intersection of the shock and the interface and $\mathscr{L} = O(1)$ corrects for the mismatch of the streamlines at the explosive/inert interface. To first order, we are justified in applying (5.7) at r^*.

A straightforward integration of (4.8) yields the following:

$$\alpha = 0: \qquad \frac{dw}{dx} = -l^{1-n} \hat{\omega} \tan(\hat{\omega} x), \tag{5.8a}$$

$$\alpha = 1: \qquad \frac{dw}{dx} = -l^{1-n} \hat{\omega} J_1(\hat{\omega} x)/J_0(\hat{\omega} x), \tag{5.8b}$$

where J_0 and J_1 are Bessel functions; we have introduced the scaled variables

$$(w, x) = \left[\frac{(\gamma^2 - 1)^2}{2\gamma^2} \frac{k}{D_{cj}}\right] (z_s, r) \tag{5.9}$$

and

$$\hat{\omega}^2 = \hat{\kappa} l^{n-1}. \tag{5.10}$$

Requiring that equations (5.8a) and (5.8b) satisfy (5.7) at $r = r^*$, we get two transcendental equations relating the detonation velocity, l, to the half-size of the explosive

charge. Solving these equations, we get the diameter-effect relation for plane-symmetric and axisymmetric geometries:

$$\alpha = 0: \qquad |z_s'(r^*)| = l^{1-n}\hat{\omega}\tan(\hat{\omega}x^*); \tag{5.11a}$$

$$\alpha = 1: \qquad |z_s'(r^*)| = l^{1-n}\hat{\omega}J_1(\hat{\omega}x^*)/J_0(\hat{\omega}x^*). \tag{5.11b}$$

Integrating (5.8) an additional time, we get the shock locus:

$$\alpha = 0: \qquad w = l^{1-n}\ln[\cos(\hat{\omega}x)/\cos(\hat{\omega}x^*)]; \tag{5.12a}$$

$$\alpha = 1: \qquad w = l^{1-n}\ln[J_0(\hat{\omega}x)/J_0(\hat{\omega}x^*)]. \tag{5.12b}$$

Detailed calculations of the flow near the interface (Bdzil 1976) show that the corrections to (5.12) near the interface are of the order of 10 %. Therefore, even near the interface, (5.12) provide a good approximation to the shock locus.

Analysing the functions (5.11) and (5.12), we are led to some interesting conclusions. First, multiplying (5.11) by x^* and then taking the limit as $x^* \to \infty$, we find that $\cos(\hat{\omega}x^*) \propto r^{*-1}[J_0(\hat{\omega}x^*) \propto r^{*-1}]$, so that

$$\lim_{r^*\to\infty} l = 1 - O(r^{*-2}). \tag{5.13}$$

It can be shown that (5.13) is true without regard to the form of the rate law. That is, the extrapolation to infinite charge size detonation velocity is not linear in r^{*-1}, as commonly assumed, but instead is quadratic in r^{*-1}. Second, the value of l at failure in the l *vs.* r^{*-1} plane will not in general occur at the value given by (5.2). For $n = 1$, failure occurs at the value given by (5.2) with an infinite value for the slope $dl/d(r^{*-1})$. When $n < 1$, failure continues to occur at the value given by (5.2). However, the slope $dl/d(r^{*-1})$ is finite at the failure point. With $n > 1$, failure occurs for $\hat{\kappa} < \hat{\kappa}_f$ and $l > l_f$, where $\hat{\kappa}_f$ and l_f are given by (5.2). The slope $dl/d(r^{*-1})$ at failure is infinite for this case. We can restate this result as follows: (1) for $n < 1$ detonation failure occurs first at the centre of the charge, (2) for $n > 1$ detonation failure occurs first at the edge of the charge. The magnitude of both of these effects as well as the general scale of the diameter effect depends on the size of δ (i.e. on the confinement). The effects are negligible for δ very small. When δ is larger the effects are observable but small. We must keep in mind that, near the edge of the charge, the terms which have been neglected in the calculation should be included as δ is made larger.

Figure 4 shows the diameter effect (l *vs.* z^*/r^*), where z^* is the one-dimensional reaction-zone length,

$$z^* = \frac{2\gamma D_{cj}}{(\gamma+1)^3 k}\left[\frac{-(\gamma-3)}{2(\gamma-1)} + \frac{(\gamma-1)}{(\gamma+1)}\ln\left(\frac{2\gamma}{\gamma-1}\right)\right], \tag{5.14}$$

for $\delta\mathscr{L} = 0{\cdot}098$ and for the four cases discussed in figure 3. The two sets of co-ordinates along the horizontal axis correspond to cylindrical (plane) symmetry, and the dots represent the points of detonation failure in this plane. We observe that the scaling from axisymmetric to plane-symmetric flow is a factor of two along the horizontal axis. Also, the r^{*-2} limiting behaviour near $l = 1$ and the departure from the failure condition of (5.2) are not pronounced. The value of $\delta\mathscr{L}$ considered here is close to the value for nitromethane confined in thick wall brass tubes at 34 °C ($\delta\mathscr{L} = 0{\cdot}08$). Figure 5 is similar to figure 4 except $\delta\mathscr{L} = \frac{1}{3}$. Now, the slope of the curves is distinctly horizontal near $l = 1$ and the points of detonation failure have moved up to smaller

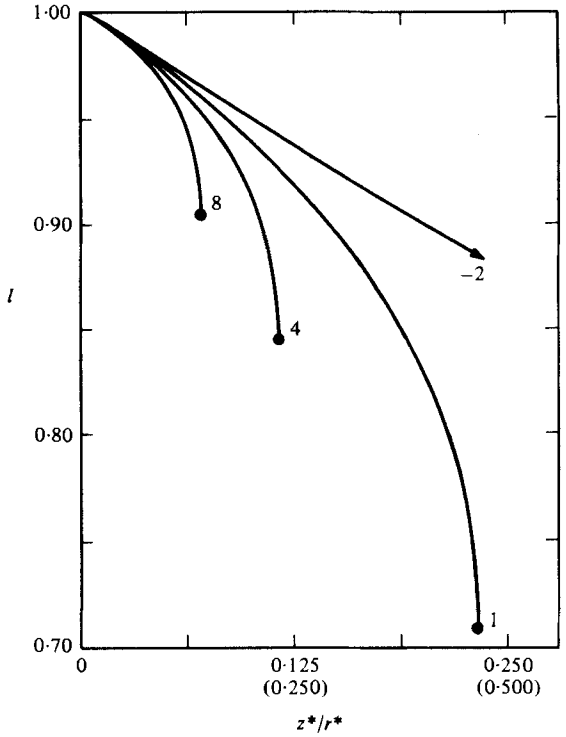

FIGURE 4. The detonation-velocity fraction (l) *vs.* the one-dimensional reaction-zone length (z^*) divided by the explosive half-size (diameter effect) for equation (4.5), with $\delta\mathscr{L} = 0{\cdot}098$, $\gamma = 3$, and $n = -2, 1, 4$ and 8. The points of detonation failure (dots) agree with equation (5.2.). Cylindrical (plane) symmetry are distinguished by the horizontal axis. The $n = -2$ curve does not show failure.

velocity deficits. Also, the scaling from axisymmetric to plane-symmetric flow is no longer a factor of two along the horizontal axis. The off-axis results for the case of cylindrical symmetry are summarized in figure 6. We note that with the exception of the largest charges, where $S^{-1} \sim r^{*-2}$, the mapping from S^{-1} to r^{*-1} essentially preserves the shape of the curves in going from l *vs.* $\hat{\kappa}$ to l *vs.* r^{*-1}. Roughly speaking, an m-fold decrease in the confinement angle is equivalent to an m-fold increase in the charge half-size.

The results for the diameter effect presented above indicate that the extrapolation to infinite charge diameter is quadratic in r^{*-1} and not linear. If we now consider the properties of the shock locus as given by (5.12), we find that this feature of the diameter effect is revealed in the shock locus as well. A convenient set of parameters to discuss the shock shape with is the distance in the z-direction from the lag to the lead point on the shock

$$y^* \equiv z\text{-distance from the lag to the lead point on the shock,}$$

and the charge half-size. Using equation (5.13) in (5.12), we find

$$\lim_{r^*\to\infty} y^* = O[\ln(r^*)]. \tag{5.15}$$

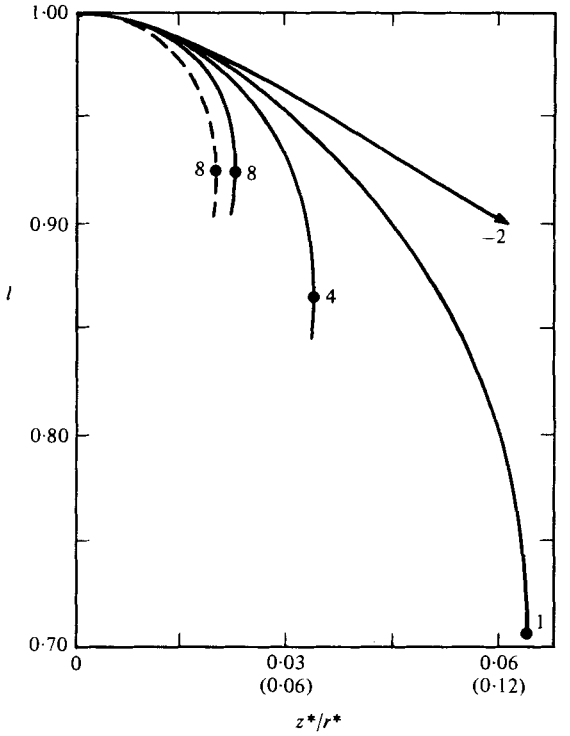

FIGURE 5. The diameter effect for $\delta\mathscr{L} = \frac{1}{3}$. See caption for figure 4 for other details. The dashed curve is for a plane-symmetric calculation, the others are for cylindrical symmetry. The dots represent the points of detonation failure and do not agree with equation (5.2).

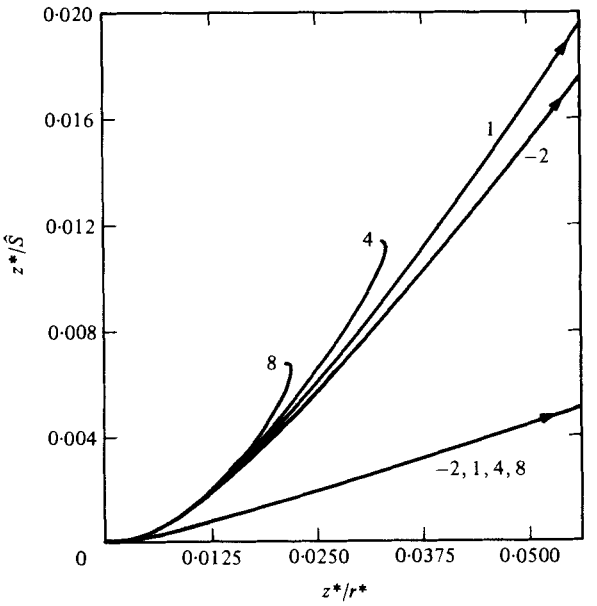

FIGURE 6. The scaled central-streamline shock curvature $(-z^*d^2z_s/dr^2)$ *vs.* the scaled inverse charge half-size (z^*/r^*). The rate law is given by equation (4.5), $\gamma = 3$, and $n = -2$, 1, 4 and 8. The arrows indicate the curves go off the graph to the right as straight lines. The symmetry is cylindrical. For the upper four curves $\delta\mathscr{L} = \frac{1}{3}$. The bottom curve has $\delta\mathscr{L} = 0{\cdot}098$.

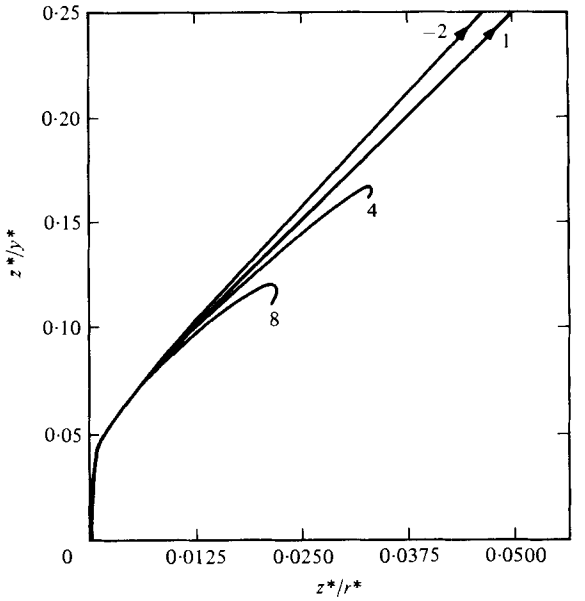

FIGURE 7. The inverse of the scaled shock lead-lag distance *vs.* the inverse of the scaled charge half-size. The rate law is given by equation (4.5), $\gamma = 3$, $\delta\mathscr{L} = \frac{1}{3}$, and $n = -2, 1, 4$ and 8. The symmetry is cylindrical. The arrows indicate the curves go off the graph to the right nearly linearly.

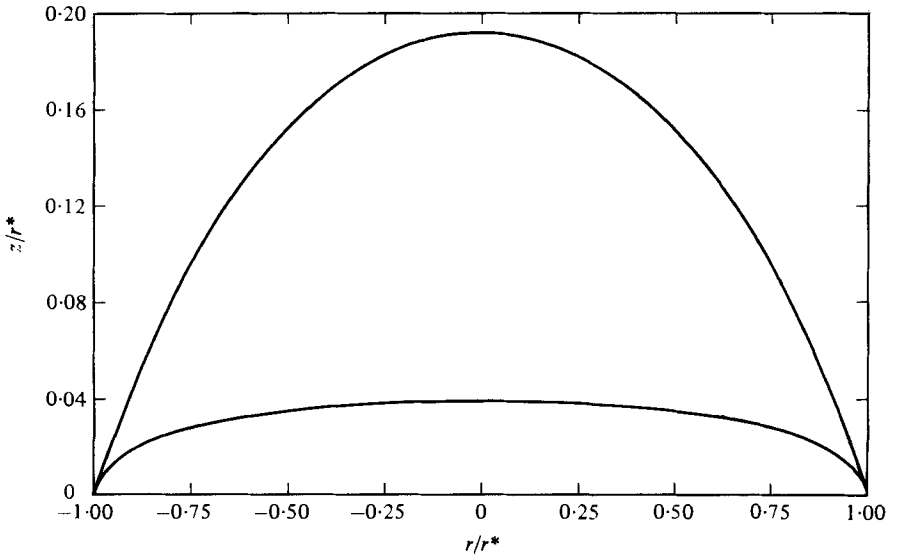

FIGURE 8. The shock loci for $l = 0{\cdot}9997$ (lower curve) and for $l = 0{\cdot}9109$ (upper curve). The symmetry is cylindrical, $\gamma = 3$, $n = 8$ and $\delta\mathscr{L} = \frac{1}{3}$.

Figure 7 shows this behaviour. That is, the distance from the lag to the lead point on the shock does not have a defined upper bound. Figure 8 compares the shock locus when $\gamma = 3$, $n = 8$, $\delta\mathscr{L} = 0{\cdot}333$, and cylindrical symmetry for a charge near infinite medium velocity $l = 0{\cdot}9997$ (lower curve) to a charge near failure velocity $l = 0{\cdot}9109$ (upper curve). Near failure the curvature is nearly constant along the entire shock.

For large charges the shock is relatively flat, with the curvature being small near the centre and increasing as the edge is approached. Thus, the shock locus experiences a qualitative change in shape with charge size.

In summary, we have shown that by generalizing the Wood–Kirkwood assumption a self-consistent reaction-zone structure for a two-dimensional detonation can be calculated. The most significant properties of this steady-state solution are:

(1) A first approximation to the radial flow is obtained.

(2) The detonation failure limit is defined for a model state-dependent rate law.

(3) The diameter effect is calculated.

(4) The shock locus is determined.

6. Comparison of theory with experiment

In the previous sections, we showed that the generalized Wood–Kirkwood assumptions lead to a mathematically consistent approximate solution of the partial differential equations governing two-dimensional steady-state reactive flow. The resulting theory leads to a number of conclusions which are unexpected, or at least not in keeping with the lore of the diameter effect and the related phenomena:

(1) the extrapolation of the measured detonation velocity to infinite charge size is quadratic in (charge size)$^{-1}$ and not linear as generally assumed;

(2) in the limit of infinite charge size, the flow along the central streamline is one-dimensional, while the distance from the lag to the lead point on the shock becomes infinite.

By comparing our calculations with experiment in a region where these effects are important, we will show that the theory and experiment are in substantial agreement. In order to maintain uniformity in the analysis, we will use (4.5) as the rate law even though it is probably physically unrealistic.

The available experimental data which are both of good quality and of interest for the comparison we wish to make are limited. Most of them are unpublished and are available only as private communications from personnel at the Los Alamos Scientific Laboratory. For our comparison we choose some data on nitromethane confined in thick-walled brass tubes and on PBX-9404 unconfined.

The comparison of theory and experiment for nitromethane is probably inappropriate, since the theoretical diameter-effect curve is downward concave and has an infinite slope at failure and the nitromethane curve is linear (for the experimental charge sizes). However, the available nitromethane data do not show any evidence of gross unsteady phenomena far from the failure size, and only as the failure size is approached are pronounced failure waves (instabilities which may quench the detonation) observed (Watson 1970). Therefore, it seems reasonable to assume that detonation failure in nitromethane is the result of an onset of a gross hydrodynamic instability on a steady-state two-dimensional detonation. If we restrict our attention to large-diameter explosive charges, the steady-state theory presented here should serve as an approximation to the diameter effect for nitromethane far from failure.

There is one feature of the nitromethane detonation that we have ignored. Numerous experimenters have reported results which suggest that there is a dark wave structure superimposed on the gross features of the detonation front even for large-diameter charges (Davis 1965; Dremin & Savrov 1966). However, measurements of the shock

locus for large charges show that (to within $\pm 0{\cdot}01$ mm) the shock is smooth and (to within 5 % of the central radius of curvature) reproducible (Davis 1964). Since both the shock locus and detonation velocity depend only on integrals of the net heat release along a streamline through the reaction zone, we might expect that a steady-state theory would provide some average first approximation to the diameter effect.

The data for nitromethane/brass are particularly convenient for our comparison since the streamline deflection angle at the explosive/inert boundary is quite small. Thus, our assumption of a small streamline deflection angle is certainly satisfied. The data were collected over a period of ten years by two investigators. Commercial grade nitromethane was used. The detonation velocities at 34 °C were measured using a pin technique (Malin 1955). The pins were mounted flush with the inner wall of the tube in holes drilled through the 6·35 mm tube wall. The shock loci at 25 °C were measured using a velocity synchronized smear-camera technique (Davis 1964). A mirrored glass plate (mirror toward the explosive) was attached obliquely to the end of a 3 mm thick wall brass tube. The mirror angle was selected so that the detonation wave swept the mirror at the same velocity that the image was swept on the film. Light from an external source was extinguished when the detonation wave deflected the mirror. This technique has the advantage of giving very crisp records. It is well known that nitromethane exhibits a strong temperature effect on both the infinite diameter detonation velocity and the slope of the diameter effect (Campbell, Malin & Holland 1955). Since it is not known how to adjust the data for temperature, we will use the data as given. The value of γ was obtained by using the results of Davis, Craig & Ramsay (1965). At 4 °C they give an initial density of $1{\cdot}159\,\mathrm{g\,cm^{-3}}$, a detonation velocity of $6374\,\mathrm{m\,s^{-1}}$, and a Chapman–Jouguet pressure of 12·2 GPa, which yields $\gamma = 2{\cdot}86$.

As input to the calculation we use $\gamma = 2{\cdot}86$ and the density at 34 °C, $1{\cdot}118\,\mathrm{g\,cm^{-3}}$. A Tait equation of state, calibrated to shock Hugoniot data in the region 5–25 GPa, was used for the brass. The explosive/inert match is described in detail in appendix F. A description of the mean flow in the explosive adjacent to the inert, the flow in the inert, and the explosive/inert match is given. Using equations (F 3) and (F 38), we find that for nitromethane confined by brass

$$\delta = 0{\cdot}07, \quad \mathscr{L} = 1{\cdot}14. \tag{6.1}$$

The only parameters which remain free are: the state dependence of the rate (n), the infinite-medium detonation velocity, and the one-dimensional reaction-zone length. Since the detonation velocity data show slight upward concavity, we set n to the smallest physically reasonable value, $n = -4$. This corresponds to a rate whose dependence on the shock state is nearly neutral. When $n < -4$ ($n > -4$), the rate at the shock decreases (increases) with increasing shock pressure. The remaining parameters were selected by requiring a good fit to the diameter effect data, particularly for the larger charges. We find that the one-dimensional reaction-zone length is 0·0665 mm and the one-dimensional detonation velocity is $6209\,\mathrm{m\,s^{-1}}$. Figure 9 shows the calculated diameter effect, the five data points, and the experimentally determined detonation failure point. Using this calibration the shock loci were calculated for a 25·4 mm radius charge and a 6·35 mm radius charge, and compared with the experimentally measured values at 26 °C. Figure 10 shows that the calculated and experimental values for the shock locus are in very good agreement. Thus, away from the failure point, this theory, with its unconventional features, is in good agreement

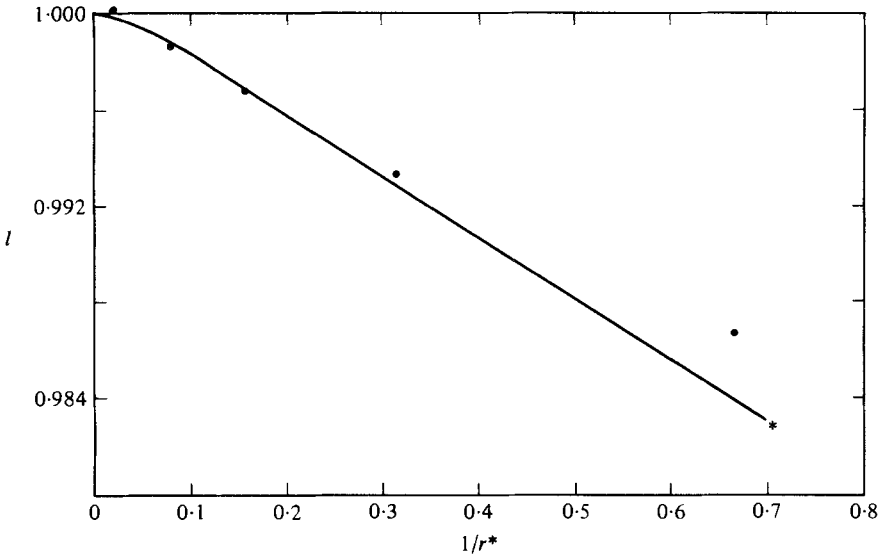

FIGURE 9. The diameter effect for nitromethane at 34 °C confined in brass cylinders of inner radius r^*. The curve is the calculation, the circles are the data points, and the star is the experimental failure point. The parameter values are: $\rho_0 = 1{\cdot}118$ g cm^{-3}, $\gamma = 2{\cdot}86$, $D_{cj} = 6209$ m s^{-1}, $n = -4$, and the one-dimensional reaction-zone length = 0·0665 mm.

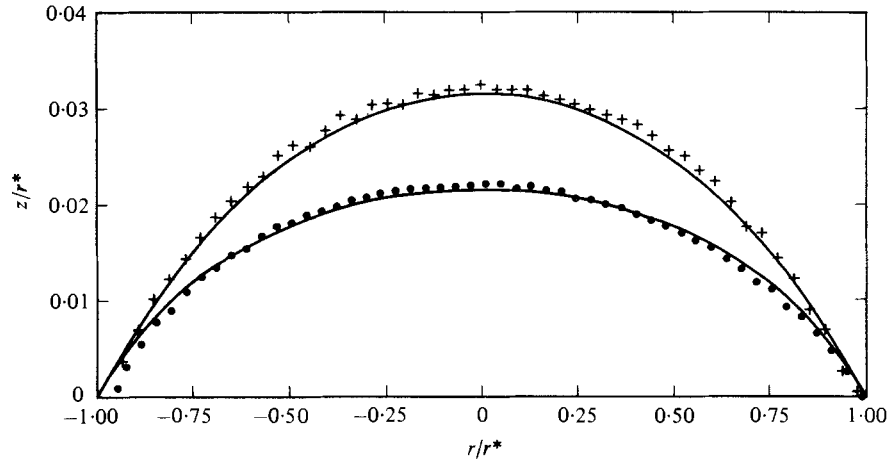

FIGURE 10. The shock loci for nitromethane confined in brass cylinders. The curves are the calculation, the circles are the 25·4 mm radius data, and the crosses are the 6·35 mm radius data.

with experiment. The calculation based on this theory represents the first quantitatively correct calculation of the diameter effect and shock loci that has been made.

It's worth noting that the one-dimensional reaction-zone length [equation (5.14)] determined by this calculation (0·0665 mm) is for the reaction rate [equation (4.5)].

A limited amount of data is also available for the solid explosive PBX-9404, detonated unconfined (Campbell & Engelke 1976). Since the diameter effect is strongly downward concave for this material, the theory can be calibrated to reproduce the entire curve, including the detonation failure point. Due to the lack of confinement,

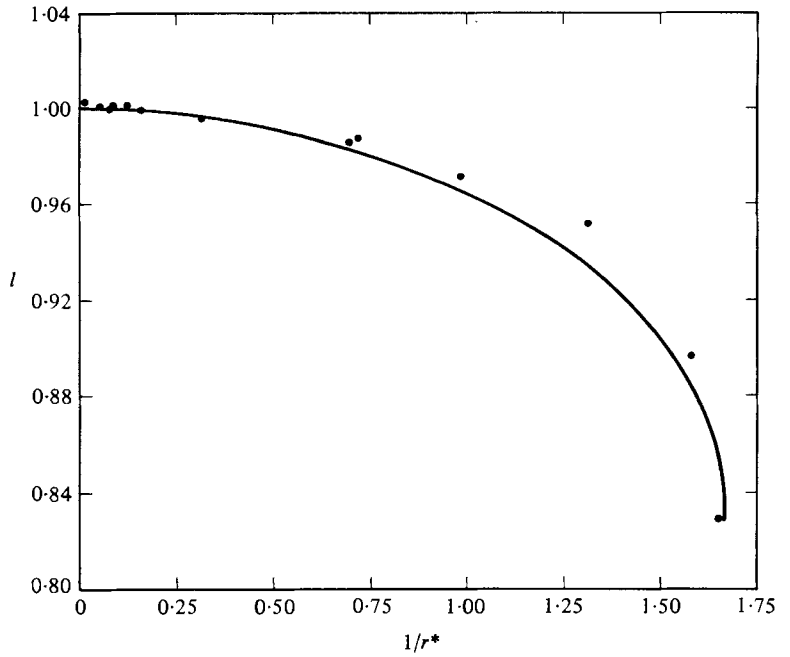

FIGURE 11. The diameter effect for unconfined cylinders of PBX-9404. The curve is the calculation, the circles are the data from Campbell & Engelke (1976). The parameter values are: $\rho_0 = 1{\cdot}84\ \mathrm{g\,cm^{-3}}$, $\gamma = 2{\cdot}95$, $D_{cj} = 8780\ \mathrm{m\,s^{-1}}$, $n = 2{\cdot}6$, and the one-dimensional reaction-zone length = 0·0220 mm.

the flow at the intersection of the shock and the charge boundary must be sonic (see appendix C). Appendix F provides no guidance on the selection of the parameter $\mathscr{L}$ for this case. However, since the flow must be subsonic as we proceed into the explosive, we will set $\mathscr{L} = 1{\cdot}0$ and take δ to be the tangent of the deflection angle at the sonic point on the shock. The value of δ is larger for this case than in the previous example. This provides us with a test of both the usefulness of the small deflection angle approximation as well as exaggerating the large-radius charge features of this model.

Calibrating the model to this system is particularly easy. The initial density is $1{\cdot}84\,\mathrm{g\,cm^{-3}}$ and the polytropic exponent is $\gamma = 2{\cdot}95$ (Davis 1976). Requiring the flow at the shock to be sonic at the edge and subsonic elsewhere, (3.6) and (5.7) give us

$$\delta = 0{\cdot}36, \quad \mathscr{L} = 1{\cdot}0. \tag{6.2}$$

If the failure point is to be reproduced, we must take $n = 2{\cdot}6$ and the one-dimensional reaction-zone length to be 0·0220 mm. Finally, the best fit to the large-diameter detonation velocities is obtained when $D_{cj} = 8780\ \mathrm{m\,s^{-1}}$. Figure 11 compares the calculated diameter effect with the experimental data. Generally, the agreement is good. The relatively flat diameter effect for large charges predicted by this model is consistent with the data. Near the knee of the curve the agreement could be better. In large part this is due to the relatively weak state dependence of the rate given by (4.5). Shock locus data exist only for the 12·7 mm radius experiment. Figure 12 shows that the calculated and experimental shock loci are in excellent agreement. The very good agreement of calculation and experiment near the charge boundary adds support to our small-deflection-angle approximation. Also, the overall agreement of the shock

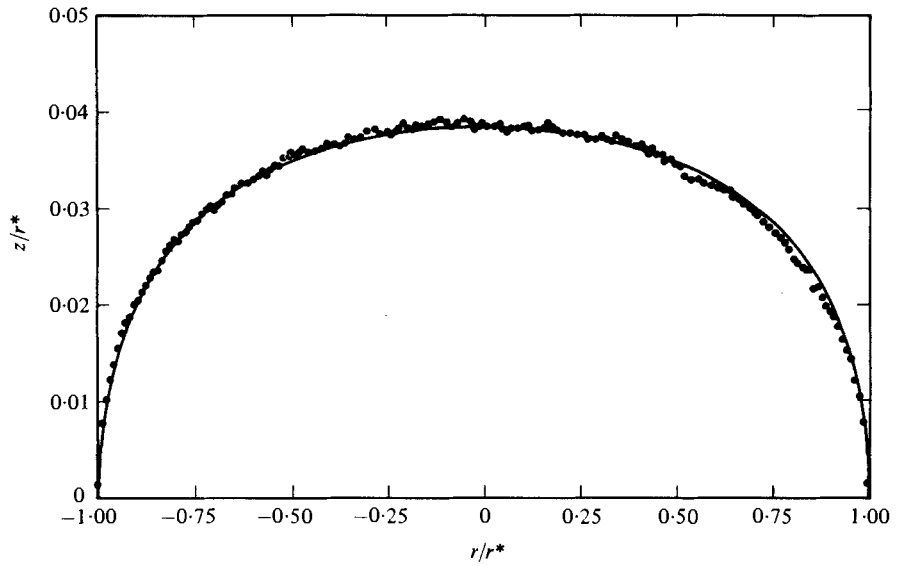

FIGURE 12. The shock locus for a 12·7 mm radius unconfined PBX-9404 cylinder. The curve is the calculation, the circles are the data discussed in Campbell & Engelke (1976).

locus for a charge whose detonation velocity is on the nearly horizontal portion of the diameter effect, provides some measure of support for the features of this theory at large charge size.

Considering the simplicity of the model, the good agreement of theory with experiment is perhaps surprising. To place these results in proper perspective, we need to reflect on the following points. First, the shock shapes and velocities do not uniquely define the flow. It can be shown that the local curvature of the shock (shock shape) depends only on the integral of the heat release along the local streamline and not on the local rate. This is true even very near the explosive/inert interface. Second, the sensitivity of the rates to local shock state is either not great (e.g. for PBX-9404 the rate depends only weakly on the state) or not tested by the experiment (e.g. for nitromethane/brass the variation of pressure along the shock is small). Thus, even the dependence of the rates on local shock state is not tested harshly. Third, the sensitivity of the calculations to the equation of state (i.e. the shock slope at the explosive/inert interface) is not great. For nitromethene/brass, the total pressure variation along the shock is small, while for PBX-9404 the sonic condition at the edge tests the equation of state near the pressure range where it was calibrated.

In conclusion, where this theory is applicable, it is in substantial agreement with experiment.

7. Summary

The detonation diameter effect has been calculated with a steady-state theory that is a generalization of the Wood–Kirkwood theory. This theory is applicable to high-density explosives. It gives the relation between the detonation velocity and central radius of curvature of the shock and between the detonation velocity and the charge

size. The theory predicts the detonation failure state and gives the shock locus as a function of the charge size. For systems to which the theory has been applied, it reproduces experimental measurements faithfully.

Appendix A. Calculation of the order of the vorticity

One of the central assumptions of the Wood–Kirkwood theory is that the radius of curvature of the shock is large compared with the one-dimensional reaction-zone length. In this appendix we will show how this leads to the conclusion that the vorticity Ω is small.

We first give a well-known result, due to Hayes (1957). The vorticity generated by a curved shock passing into a quiescent fluid, where the fluid is governed by (2.1)–(2.4) and (2.8), is

$$\Omega_+ = \frac{4D}{(\gamma^2-1)} z_s' z_s'' [1+(z_s')^2]^{-2}, \tag{A 1}$$

for a two-dimensional plane or axisymmetric flow, where Ω_+ is the vorticity just behind the shock. Therefore, if the radius of curvature of the shock is large

$$\{S^{-1} = -z_s''[1+(z_s')^2]^{-\frac{3}{2}}\}$$

measured in units of the one-dimensional reaction-zone length, then the vorticity at the shock $[O(\delta S^{-1})]$ is small.

Using equations (2.1)–(2.3), we can derive an equation that describes the evolution of the vorticity behind the shock. We begin by introducing the vector identity

$$\mathbf{u}.\nabla\mathbf{u} = (\nabla\times\mathbf{u})\times\mathbf{u} + \tfrac{1}{2}\nabla(\mathbf{u}.\mathbf{u}). \tag{A 2}$$

Substituting equation (2.2) into (A 2), we get

$$(\nabla\times\mathbf{u})\times\mathbf{u} = -\frac{1}{\rho}\nabla P - \tfrac{1}{2}\nabla(\mathbf{u}.\mathbf{u}). \tag{A 3}$$

Taking the curl of this equation and recalling that

$$\nabla.\nabla\times\mathbf{u} = 0,$$

and for our two-dimensional flow

$$(\nabla\times\mathbf{u}).\nabla\mathbf{u} = 0,$$

we get

$$\mathbf{u}.\nabla\boldsymbol{\Omega} + \boldsymbol{\Omega}\nabla.\mathbf{u} = -\nabla\rho^{-1}\times\nabla P. \tag{A 4}$$

Substituting equation (2.1) into the above equation, gives us the desired result

$$\mathbf{u}.\nabla(\Omega\rho^{-1}) = -\rho^{-1}\nabla\rho^{-1}\times\nabla P. \tag{A 5}$$

The order of the source term in (A 5) can easily be found. Transforming from the independent variables (z,r) to the more suitable variables (λ, z_s'), the source term becomes

$$-\rho^{-1}\frac{\partial\lambda}{\partial z}\frac{d^2z_s}{dr^2}\left[\frac{\partial\rho^{-1}}{\partial\lambda}\frac{\partial P}{\partial z_s'} - \frac{\partial\rho^{-1}}{\partial z_s'}\frac{\partial P}{\partial\lambda}\right]. \tag{A 6}$$

Since the deviations from the one-dimensional solution are $O(\delta)$, it follows that the source term for vorticity production in the flow is $O(\delta S^{-1})$. Therefore, we find that

$$\Omega = O(\delta S^{-1}). \tag{A 7}$$

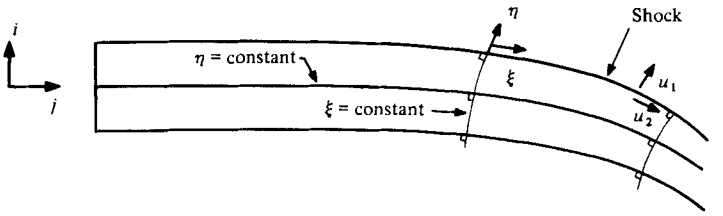

FIGURE 13. The shock-oriented, orthonormal, curvilinear co-ordinates we will use in our analysis.

Appendix B. Calculation of the streamline curvature

The derivation of the generalized Wood–Kirkwood theory requires that we give some information about u_r. In this appendix we will show how a differential equation for the streamline deflection can be derived from (2.1)–(2.4) and (2.8). The starting point for the analysis is the identity

$$\frac{\partial}{\partial z}\left(\frac{u_r}{u_z}\right) = \frac{\Omega}{u_z} - \left(\frac{u_r}{u_z^2}\right)(\nabla.\mathbf{u})_{\text{plane}} + \frac{\partial(\mathbf{u}.\mathbf{u})}{\partial r}\Big/(2u_z^2), \tag{B 1}$$

where $(\nabla.\mathbf{u})_{\text{plane}} = \partial u_z/\partial z + \partial u_r/\partial r$. The analysis is most conveniently carried out in the plane curvilinear co-ordinates shown in figure 13.

As an alternative to carrying all the terms in the analysis of (B 1), we will neglect derivatives in the ξ direction since they are $O(\delta S^{-1})$, and simply quote the results for an inert flow relating streamline curvature at the shock to the vorticity for a two-dimensional plane or axisymmetric flow. For an inert polytropic fluid that is quiescent ahead of the shock, we have in the strong shock approximation (Rao 1973)

$$\left(\frac{d^2z}{dr^2}\right)_+ = -\frac{2(\gamma-1)}{D}\frac{(u_+^2 - c_+^2)}{u_{z+}^2}\Omega_+ + \frac{\alpha}{r}\left(\frac{u_{r+}}{u_{z+}}\right)^2, \tag{B 2}$$

where $(d^2z/dr^2)_+$ is the streamline curvature at the shock. Therefore, for a convex shock (as perceived by a shock-fixed observer looking toward the quiescent material) the streamlines curve away from the central streamline in subsonic regions of the flow.

We begin our analysis by giving the expressions for the divergence and gradient operators in our plane curvilinear co-ordinates (Morse & Feshbach 1953)

$$\nabla.\mathbf{F} = f^{-1}(1-f^2)^{-\frac{1}{2}}\left[\frac{\partial(F_1 f)}{\partial\eta} + \frac{\partial[F_2(1-f^2)^{\frac{1}{2}}]}{\partial\xi}\right], \tag{B 3}$$

$$\nabla\phi = \boldsymbol{\eta}(1-f^2)^{-\frac{1}{2}}\frac{\partial\phi}{\partial\eta} + \boldsymbol{\xi}f^{-1}\frac{\partial\phi}{\partial\xi}, \tag{B 4}$$

where
$$f = z_s'[1+(z_s')^2]^{-\frac{1}{2}} \tag{B 5}$$

and
$$\mathbf{i} = (1-f^2)^{\frac{1}{2}}\boldsymbol{\eta} + f\boldsymbol{\xi}, \tag{B 6}$$

$$\mathbf{j} = -f\boldsymbol{\eta} + (1-f^2)^{\frac{1}{2}}\boldsymbol{\xi}. \tag{B 7}$$

Using the definitions given in (B 1), we write

$$\xi-\eta = z_s+\int\frac{dr}{z_s'} = h^{-1}(r), \tag{B 8}$$

so that

$$\frac{\partial f}{\partial\eta} = -z_s''(1-f^2)^{\frac{3}{2}}h', \tag{B 9}$$

$$\frac{\partial(1-f^2)^{\frac{1}{2}}}{\partial\xi} = -z_s''f(1-f^2)h', \tag{B 10}$$

and

$$h' = f(1-f^2)^{\frac{1}{2}}. \tag{B 11}$$

Therefore, equations (B 3) and (B 4) can be written as

$$\nabla.\mathbf{F} = (1-f^2)^{-\frac{1}{2}}\frac{\partial F_1}{\partial\eta}+(1-f^2)^{\frac{1}{2}}\left(\frac{\partial F_2}{\partial r}\right)_{\eta,\,z=\eta+z_s} - z_s''[(1-f^2)^{\frac{3}{2}}F_1+f(1-f^2)F_2], \tag{B 12}$$

and

$$\mathbf{j}.\nabla\phi = -f(1-f^2)^{-\frac{1}{2}}\frac{\partial\phi}{\partial\eta}+(1-f^2)\left(\frac{\partial\phi}{\partial r}\right)_{\eta,\,z=\eta+z_s}. \tag{B 13}$$

To get an expression for $(\nabla.\mathbf{u})_{\text{plane}}$ in (B 1) that is useful for computation, we need to replace $\partial u_1/\partial\eta$ by $\partial(\mathbf{u}.\mathbf{u})/\partial\eta$. Some straightforward algebra yields the identity

$$\mathbf{u}.\mathbf{u}\frac{\partial u_1}{\partial\eta} = \tfrac{1}{2}u_1\frac{\partial(\mathbf{u}.\mathbf{u})}{\partial\eta}-u_2u_z^2\frac{\partial}{\partial\eta}\left(\frac{u_r}{u_z}\right)+u_2(\mathbf{u}.\mathbf{u})z_s''f(1-f^2)^{\frac{3}{2}}, \tag{B 14}$$

so that

$$\begin{aligned}(\nabla.\mathbf{u})_{\text{plane}} = {}& \tfrac{1}{2}u_1(1-f^2)^{-\frac{1}{2}}(\mathbf{u}.\mathbf{u})^{-1}\frac{\partial(\mathbf{u}.\mathbf{u})}{\partial\eta}-u_2u_z^2(1-f^2)^{-\frac{1}{2}}(\mathbf{u}.\mathbf{u})^{-1}\frac{\partial}{\partial\eta}\left(\frac{u_r}{u_z}\right)\\ &+(1-f^2)^{\frac{1}{2}}\left(\frac{\partial u_2}{\partial r}\right)_{\eta,\,z=\eta+z_s}-u_1z_s''(1-f^2)^{\frac{3}{2}}.\end{aligned} \tag{B 15}$$

Equation (2.5) gives us a second equation relating $(\nabla.\mathbf{u})_{\text{plane}}$ and $\partial(\mathbf{u}.\mathbf{u})/\partial\eta$

$$(\nabla.\mathbf{u})_{\text{plane}}+\frac{\alpha u_r}{r} = [\tfrac{1}{2}\mathbf{u}.\nabla(\mathbf{u}.\mathbf{u})+qR/(\rho e_p)]c^{-2}, \tag{B 16}$$

where

$$\mathbf{u}.\nabla(\mathbf{u}.\mathbf{u}) = u_1(1-f^2)^{-\frac{1}{2}}\frac{\partial(\mathbf{u}.\mathbf{u})}{\partial\eta}+u_2(1-f^2)^{\frac{1}{2}}\left[\frac{\partial(\mathbf{u}.\mathbf{u})}{\partial r}\right]_{\eta,\,z=\eta+z_s} \tag{B 17}$$

Combining equations (B 15)–(B 17), we can solve for $(\nabla.\mathbf{u})_{\text{plane}}$ and $\partial(\mathbf{u}.\mathbf{u})/\partial\eta$ in terms of the rate, streamline curvature, and various derivatives taken tangent to the shock. In turn, equation (B 13) can be used to express $\partial(\mathbf{u}.\mathbf{u})/\partial r$ in terms of the same quantities. The right-hand side of (B 1) is

$$\frac{\partial}{\partial z}\left(\frac{u_r}{u_z}\right) = \frac{\partial}{\partial\eta}\left(\frac{u_r}{u_z}\right)+f(1-f^2)^{\frac{1}{2}}\left[\frac{\partial}{\partial r}\left(\frac{u_r}{u_z}\right)\right]_{\eta,\,z=\eta+z_s} \tag{B 18}$$

To complete our analysis all we need do is recognize that every derivative taken in the ξ direction is proportional to $z_s'' = O(S^{-1})$. Therefore, we find that (B 1) becomes

$$\frac{\partial}{\partial z}(u_r/u_z) = \frac{u_2qR(1-f^2)^{\frac{1}{2}}}{u_z^2(u_1^2-c^2)\rho e_p}+O[(u_r/u_z)S^{-1}]. \tag{B 19}$$

This is an interesting result. It states that in regions of subsonic flow an exothermic reaction curves the streamlines toward the symmetry axis of the flow. Recalling (B 2),

we find that near the shock in a subsonic flow the shock curvature acts to curve the streamlines away from the symmetry axis while an exothermic reaction curves the streamlines toward the symmetry axis. Therefore, if the radius of curvature of the shock is large, the dominant effect will be due to the chemical reaction and the curvature of the streamlines will be inward.

Appendix C. Discussion of the flow at the edge of the explosive

In this paper we will not be overly interested in the boundary conditions along the edge of the explosive charge. For the sake of completeness, however, this appendix briefly describes the flow in the vicinity of the intersection of the charge boundary and the shock. We will only consider the case of two-dimensional planar symmetry.

For this analysis, it is most convenient to use a set of polar co-ordinates centred at the intersection of the shock and the explosive-charge boundary. We then assume that all of the flow variables can be expanded as Taylor series in τ, where τ is the radial co-ordinate

$$\lambda = \tau\lambda^{(1)}(\theta) + \ldots, \tag{C 1}$$

$$u_z = u_z^{(0)}(\theta) + \tau u_z^{(1)}(\theta) + \ldots, \tag{C 2}$$

etc.

Transforming equations (2.1)–(2.4) and (2.8), and the desired rate law to polar co-ordinates, and then substituting (C 1)–(C 2) into the result gives us a hierarchy of ordinary differential equations for the θ dependence of the solution. Finding solutions to the resulting equations is straightforward, although somewhat time-consuming. We will not display the calculation here, but instead simply present the results for the example of greatest interest, an unconfined detonation.

The lowest-order equations are those for an inert flow. Solutions can be found in Courant & Friedrichs (1948). Three cases come up: the flow at the detonation shock is (1) subsonic, (2) supersonic or (3) exactly sonic. Case (1) is ruled out because the analyticity requirements of subsonic flows do not permit the flow to be both subsonic (shock) and supersonic (zero pressure streamline) at the same point. Case (2) does allow the pressure to drop from a finite value at the shock to zero at the outermost streamline via a Prandtl–Meyer singularity. However, for this case information about the charge boundary can influence only a very limited region of the flow, and the shock is unaware of the existence of the charge boundary. Case (3) allows both a Prandtl–Meyer singularity and propagates information about the charge boundary to the sonic locus of the flow. Therefore, we assume that the flow at the shock at the charge boundary is exactly sonic.

Extending the calculation to the next order incorporates the effects of reactivity into the flow. The results of the first two orders of the calculation, for a shock that is sonic at the edge, are shown in figure 14. It is clear that information about the charge boundary travels along the C_+ characteristics that are shown, and is deposited on the $O(1)$-sonic locus. This information is then used as data in the calculation of the subsonic flow regime, including the shock locus, detonation velocity, etc. Therefore, we can see how information about the edge propagates into and influences the entire subsonic reactive region.

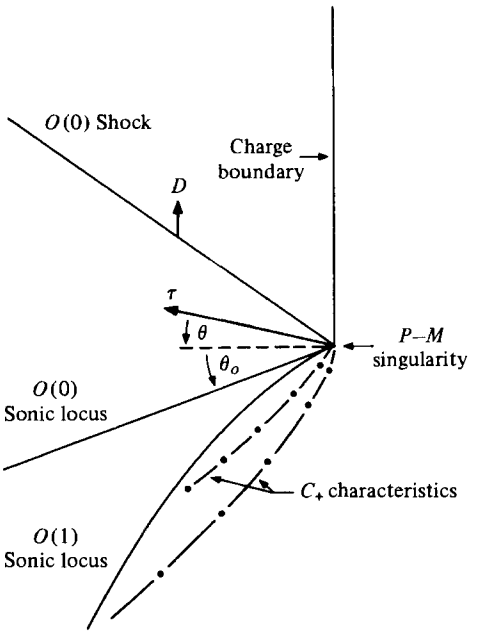

FIGURE 14. A plot of the $O(1)$ sonic locus for $\gamma = 3$ and $(\theta - \theta_0)$ small. Also shown is a schematic representation of some C_+ characteristics emanating from the Prandtl–Meyer singularity.

As we proceed into the charge we expect the flow to be less strongly influenced by the charge boundary. That is, we expect that the shock locus, the end of the reaction zone, and sonic locus will all be parallel, so that the $O(1)$-sonic locus shown in figure 14 must eventually show an inflection point. This implies that there exists one C_+ characteristic, the limiting characteristic, which is exactly tangent to the sonic locus. All of the C_+ characteristics to the right of it do not influence the subsonic flow regime. Therefore, as we introduce confinement into the problem, the subsonic flow regime will remain unchanged until the confinement becomes sufficiently heavy so as to influence the limiting characteristic. As the confinement is increased further, a point is reached when the flow in the explosive becomes subsonic and analytic in this entire region.

A more detailed discussion of confinement can be found in Bdzil (1976).

Appendix D. Calculation of a higher-order approximation to u_r

In § 3 of this paper an equation for u_r is presented that is valid up to $O(\delta)$. Since this expression essentially defines the two-dimensional character of our problem, we will present some results which support its use.

The source for these results is a singular perturbation analysis of (2.1), (2.2), (2.3), (2.4) and (2.8) subject to all of the boundary conditions, for the rate law

$$R = k(P/P_{cj})^n t, \tag{D 1}$$

where $t = (1-\lambda)^{\frac{1}{2}}$. The sole perturbation parameter is the streamline deflection angle δ, the pair of independent variables is $(t, \bar{r} \equiv \delta r)$, and the expansions taken for the

	$M(t)$		
t	$n = 1$	$n = 4$	$n = 8$
1·00	0·00	0·00	0·00
0·75	−0·02	0·16	0·10
0·50	−0·27	0·22	0·22
0·25	−0·80	−0·01	0·26
0·00	−1·71	−1·11	−0·84

TABLE 1. The $O(\delta^3)$ corrections to the central streamline flow divergence.

dependent variables and the detonation velocity are

$$u_z^2 = \left(\frac{D_{cj}}{\gamma+1}\right)^2 [(\gamma-t)^2 + \delta^2\psi + \ldots], \tag{D 2}$$

$$P = \frac{\rho_0 D_{cj}^2}{\gamma+1}[(1+t) + \delta^2\phi + \ldots], \tag{D 3}$$

$$u_r = -\delta\frac{D_{cj}}{\gamma+1}\left[\frac{dz_s}{d\bar{r}}(1+t) - \delta^2\theta + \ldots\right], \tag{D 4}$$

$$c^2 = \left(\frac{\gamma D_{cj}}{\gamma+1}\right)^2 [(\gamma-t)(1+t)/\gamma + O(\delta^2)], \tag{D 5}$$

$$\lambda = \lambda^{(0)} + \delta^2\lambda^{(2)} + \ldots, \tag{D 6}$$

and

$$\frac{D}{D_{cj}} = 1 - \delta^2\Gamma. \tag{D 7}$$

Briefly, the leading term in (D 4) is obtained from the irrotationality of the flow at lowest order and from the known one-dimensional solution. The perturbations ψ and ϕ are obtained at the next order by solving a system of linear ordinary differential equations in t with $\bar{r}$ as a parameter. At the next order, we get the equation (where we have taken $\alpha = 0$ and restricted attention to the central streamline)

$$\frac{\partial^3\theta}{\partial t^2\,\partial\bar{r}} = \frac{\partial^2\phi}{\partial t^2}\frac{d^2z_s}{d\bar{r}^2} + \frac{2D_{cj}}{k(\gamma+1)}(1+t)^{-n}\left\{n(1+t)\left(\frac{d^2z_s}{d\bar{r}^2}\right)^2 - \frac{(\gamma-t)^{-1}}{2}\frac{\partial^2\psi}{\partial\bar{r}^2} + \frac{2n(\gamma-t)}{(1+t)}\frac{\partial^2\phi}{\partial\bar{r}^2} - \frac{\partial^3[(\gamma-t)\phi]}{\partial\bar{r}^2\,\partial t}\right\}, \tag{D 8}$$

which becomes a quadrature for $(\partial\theta/\partial\bar{r})$ when ψ and ϕ are substituted into its right-hand side. Performing the integrations on t, we get

$$\frac{\partial u_r}{\partial r} = -\frac{D}{(\gamma+1)}(1+t)\frac{d^2z_s}{dr^2} + \delta^2\frac{D_{cj}}{(\gamma+1)}M(t)\,\epsilon\frac{d^2z_s}{dr^2}, \tag{D 9}$$

where ϵ is defined in (5.1 c) and $M(t)$, which represents the deviation from (3.10), is given in table 1 for $\gamma = 3$, $\alpha = 0$, and several values of n. It can be shown that the detonation characteristics such as the wave front curvature and detonation velocity depend on the mean value of the flow divergence

$$\int_0^1 (1+t)^{1-n}\begin{Bmatrix}(1+t)\\ M(t)\end{Bmatrix}dt, \tag{D 10}$$

and experience only 1 % changes when $M(t)$ is added to the calculation.

Appendix E. Calculation of equation (3.14)

The partial differential equation (2.5) can be transformed into an ordinary differential equation which closely approximates its behaviour, and has u_z as the dependent variable, t as the independent variable, and r as a parameter. This can be accomplished by using (3.10), (3.11), (3.12), (3.13) and (2.7).

We begin by first transforming from the independent variable pair (z, r) to the pair (t, r). Equation (3.12) is the rate law. Neglecting the radial velocity in (3.12), we get a first approximation to t as a function of z and r

$$t = F(z_s - z) + O(\delta^2) + O(S^{-1}), \tag{E 1}$$

where $F(\ )$ is a known function. Differentiating (E 1) with respect to r, we get (3.13),

$$\frac{\partial t}{\partial r} = -z_s' \frac{\partial t}{\partial z} + O(\delta^3) + O(\delta S^{-1}), \tag{E 2}$$

which, when substituted into (3.12), gives

$$\left(\frac{\partial t}{\partial z}\right)_r = -\frac{R}{2tu_z}[1 - (u_r/u_z)\, z_s']^{-1} + O(\delta^4) + O(\delta^2 S^{-1}), \tag{E 3}$$

and

$$\left(\frac{\partial t}{\partial r}\right)_z = -z_s' \left(\frac{\partial t}{\partial z}\right)_r + O(\delta^5) + O(\delta^3 S^{-1}). \tag{E 4}$$

Equations (E 3) and (E 4) can be used in the operators

$$\left(\frac{\partial}{\partial z}\right)_r = \left(\frac{\partial t}{\partial z}\right)_r \frac{\partial}{\partial t} \quad \text{and} \quad \left(\frac{\partial}{\partial r}\right)_z = \left(\frac{\partial}{\partial r}\right)_t + \left(\frac{\partial t}{\partial r}\right)_z \frac{\partial}{\partial t}, \tag{E 5}$$

to make the change of variables in (2.5).

In the interest of simplicity, we will first present the central streamline (i.e. $u_r = 0$) form of (2.5). Using the equations in this appendix and (3.10), (2.5) specialized to the central streamline is

$$(\hat{c}^2 - u_z^2)\frac{du_z^2}{dt} - 4tu_z^2 \hat{c}^2 D(1+\alpha)[\hat{S}R(\gamma+1)]^{-1}(1+t) + 2tu_z^2 D_{cj}^2(\gamma+1)^{-1} = O(\hat{S}^{-2}), \tag{E 6}$$

where $\hat{S}^{-1}$ is the value of $-z_s''$ on the central streamline, and

$$\hat{c}^2 = \frac{(\gamma-1)}{2}\left[D^2 + \frac{D_{cj}^2}{(\gamma^2-1)}(1-t^2) - u_z^2\right]. \tag{E 7}$$

We can obtain an approximation to (2.5) away from the central streamline by retaining the $O(\delta^2)$ terms in (2.5) and adding them to (E 6)

$$(\hat{c}^2 - u_z^2)\frac{du_z^2}{dt} + 4tu_z^2 \hat{c}^2 D[R(\gamma+1)]^{-1}\left(z_s'' + \frac{\alpha}{r} z_s'\right)(1+t) + 2tu_z^2 D_{cj}^2(\gamma+1)^{-1}$$
$$= D_{cj}^4(\gamma+1)^{-3}(z_s')^2 f(t)/2 + O(\delta^4) + O(\delta^2 S^{-1}) + O(S^{-2}), \tag{E 8}$$

where

$$f(t) = 2(\gamma - t)(1+t)[(1+t) + 2(\gamma - t)], \tag{E 9}$$

and $\hat{c}^2$ is given by (E 7). In obtaining $f(t)$, u_z^2, $\hat{c}^2$ and D have been replaced by their one-dimensional values.

Appendix F. Calculation of the flow near the explosive/inert interface

Although we are not interested in the details of the reactive flow near the charge boundary, we must be able to convert equation-of-state information on the confining inert into the parameters for our explosive calculation. We will restrict our attention to inerts which give strong confinement of the explosive. For such materials, the weak shock approximation can be used to get a good first approximation to the inert flow.

We begin by considering the inert flow. Although it is not a necessary simplification, we use a Tait equation of state for the inert. The independent variables will be the vertical co-ordinate z and the stream function Ψ. We measure the particle velocities u_I in units of the Chapman–Jouguet detonation velocity D_{cj}, the density ρ_I in units of the initial density of the inert ρ_{0I}, and the pressure P_I in units of $\rho_{0I} D_{cj}^2$. Written in terms of these scaled variables, the shock conditions are

$$\hat{u}_{r+} = -\left(\frac{dz_s}{dr}\right)_I \hat{P}_+, \tag{F 1}$$

$$\hat{u}_{z+} = -1 + \hat{P}_+, \tag{F 2}$$

$$\tan(\theta_+) = -\left(\frac{dz_s}{dr}\right)_I \hat{P}_+ (1-\hat{P}_+)^{-1}, \tag{F 3}$$

$$\hat{\rho}_+^{-1} = \frac{n-1}{n+1} + \left(\frac{2}{n+1}\right)^2 n\hat{a}\left(\frac{2n\hat{a}}{n+1} + \hat{P}_+\right)^{-1}, \tag{F 4}$$

and

$$\left(\frac{dz_s}{dr}\right)_I^2 = -1 + \frac{2}{n+1}\left(\frac{2n\hat{a}}{n+1} + \hat{P}_+\right)^{-1}, \tag{F 5}$$

where $\hat{a}$ and n are the constants for the Tait isentrope

$$(\hat{P} + \hat{a})\,\hat{\rho}^{-n} = \text{constant}. \tag{F 6}$$

If we restrict our attention to streamline deflection angles of $O(\delta)$, then from (F 3) and (F 5) we are led to

$$\hat{P} = O(\delta). \tag{F 7}$$

That is, a small deflection angle in the inert is synonymous with a weak shock.

The governing Euler equations for the assumed planar flow are (Van Dyke 1975)

$$\frac{\partial r}{\partial z} = \frac{\hat{u}_r}{\hat{u}_z}, \quad \frac{\partial r}{\partial \hat{\Psi}} = -\frac{1}{\hat{\rho}\hat{u}_z}, \tag{F 8), (F 9}$$

$$\frac{\partial \hat{u}_r}{\partial z} - \frac{\partial \hat{P}}{\partial \hat{\Psi}} = 0, \quad (\hat{P} + \hat{a})\,\hat{\rho}^{-n} = \hat{f}(\hat{\Psi}), \tag{F 10), (F 11}$$

and

$$\frac{\hat{c}^2}{(n-1)} + \tfrac{1}{2}|\hat{\mathbf{u}}|^2 - \frac{n\hat{a}}{(n-1)} = \tfrac{1}{2}, \tag{F 12}$$

where $\hat{\Psi} = -\Psi/\rho_{0I} D_{cj}$, $\hat{c}^2$ is the scaled sound speed squared c^2/D_{cj}^2, and r is the lateral distance. We assume that the dependent variables can be expanded as

$$\hat{P} = \delta\hat{P}^{(1)} + \ldots, \quad \hat{u}_z = \hat{u}_z^{(0)} + \delta\hat{u}_z^{(1)} + \ldots, \tag{F 13), (F 14}$$

$$\hat{u}_r = \delta\hat{u}_r^{(1)} + \ldots, \quad r = r^{(0)} + \delta r^{(1)} + \ldots, \tag{F 15), (F 16}$$

$$\hat{\rho} = \hat{\rho}^{(0)} + \delta\hat{\rho}^{(1)} + \ldots, \quad \hat{c} = \hat{c}^{(0)} + \delta\hat{c}^{(1)} + \ldots, \tag{F 17), (F 18}$$

and do a regular perturbation solution of (F 8)–(F 12) subject to the shock conditions (F 1)–(F 5). At zeroth order the solution everywhere in the flow is equal to the shock (straight line) state. At first order the differential equations reduce to the wave equation

$$\left(\frac{\hat{u}_z^{(0)2}}{\hat{c}^{(0)2}}-1\right)\frac{\partial^3 r^{(1)}}{\partial z^2}=(\hat{\rho}^{(0)}\hat{u}_z^{(0)})\frac{\partial^2 r^{(1)}}{\partial \hat{\Psi}^2}, \tag{F 19}$$

where

$$u_r^{(1)}=u_z^{(0)}\frac{\partial r^{(1)}}{\partial z}, \tag{F 20}$$

$$\hat{P}^{(1)}=\hat{u}_z^{(0)}(\hat{\rho}^{(0)}\hat{u}_z^{(0)})\left(\frac{\hat{u}_z^{(0)2}}{\hat{c}^{(0)2}}-1\right)\frac{\partial r^{(1)}}{\partial \hat{\Psi}}, \tag{F 21}$$

and

$$\hat{P}^{(1)}=-\hat{\rho}^{(0)}\hat{u}_z^{(0)}\hat{u}_z^{(1)}. \tag{F 22}$$

Solving equation (F 19) and applying the shock conditions, we find

$$\hat{P}^{(1)}=-(\hat{\rho}^{(0)}\hat{u}_z^{(0)})\left(\frac{\hat{u}_z^{(0)2}}{\hat{c}^{(0)2}}-1\right)^{-\frac{1}{2}}\hat{u}_r^{(1)}, \tag{F 23}$$

where $\hat{P}^{(1)}$ and $\hat{u}_r^{(1)}$ are functions only of the characteristic co-ordinate

$$\hat{\eta}\equiv\hat{\Psi}-(\hat{\rho}^{(0)}\hat{u}_z^{(0)})\left(\frac{\hat{u}_z^{(0)2}}{\hat{c}^{(0)2}}-1\right)^{-\frac{1}{2}}z. \tag{F 24}$$

Since the pressure at the inert/explosive interface must be continuous, at the interface

$$\delta\hat{P}^{(1)}=\frac{\rho_0(1+t)}{(\gamma+1)\rho_{0I}}, \tag{F 25}$$

where $t=(1-\lambda)^{\frac{1}{2}}$, ρ_0 is the initial density of the explosive, and γ is the polytropic exponent for the explosive. Using this in equation (F 23), we get the tangent of the streamline deflection angle along the inert/explosive interface

$$\frac{u_r}{u_z}=-\tan(\theta_+)\frac{(1+t)}{2}+O(\delta^2). \tag{F 26}$$

Therefore, we find that the streamline deflection angle at the interface changes more slowly through the reaction zone than it does in the interior of the explosive. Thus we must amend the explosive solution in the vicinity of the charge boundary.

We will use equations (2.5), (2.7), (2.9) and (2.11) to generate an expression that relates the interface shape to the streamline deflection one reaction-zone length into the explosive charge. To do this, we assume that when the streamline deflection angle is small the dependent variables can be written as

$$u_z=u_z^{(0)}+\delta u_z^{(1)}+\ldots, \quad u_r=\delta u_r^{(1)}+\ldots, \tag{F 27), (F 28}$$

$$c=c^{(0)}+\delta c^{(1)}+\ldots, \quad \lambda=\lambda^{(0)}+\delta\lambda^{(1)}+\ldots, \tag{F 29), (F 30}$$

and

$$D=D_{cj}+O(\delta^2), \quad \frac{dz_s}{dr}=O(\delta). \tag{F 31), (F 32}$$

Doing a regular perturbation analysis of (2.5), (2.7) and (2.9) with z and r as the independent variables, at $O(\delta)$ we get the equation

$$\frac{\partial\hat{u}_z^{(1)}}{\partial t}+\frac{\gamma}{t(\gamma-t)}\hat{u}_r^{(1)}+\frac{2\gamma D_{cj}}{(\gamma+1)^2}\frac{(\gamma-t)(1+t)}{R^{(0)}}\left(\frac{\partial\hat{u}_r^{(1)}}{\partial r}+\frac{\alpha}{r}\hat{u}_r^{(1)}\right)=0, \tag{F 33}$$

where $t = (1-\lambda)^{\frac{1}{2}}$, $R^{(0)}$ is the one-dimensional rate, and $\hat{u}_z^{(1)}$, $\hat{u}_r^{(1)}$ are the particle velocities measured in units of $D_{cj}(\gamma+1)^{-1}$. Although the vorticity is $O(\delta)$ in this region, it does not appear in this equation. The shock boundary condition, equation (2.11), requires that $\hat{u}_z^{(1)}(t=1) = 0$. At the unperturbed sonic locus ($t = 0$), $\hat{u}_z^{(1)}$ must be bounded. As we proceed into the explosive charge $\hat{u}_z^{(1)} = 0$.

Equation (F 33) is a partial differential equation in two unknowns. Without additional information via other differential equations, we cannot solve for $\hat{u}_z^{(1)}$, $\hat{u}_r^{(1)}$ in this region. However, if we neglect $(\alpha\hat{u}_r^{(1)})/r$, since r is usually large, we can integrate (F 33) with respect to r, to get

$$\frac{d\mathscr{J}}{dt} + \frac{\gamma}{t(\gamma-t)}\mathscr{J} + \frac{2\gamma D_{cj}}{(\gamma+1)^2}\frac{(\gamma-t)(1+t)}{R^{(0)}}[\hat{u}_r^{(1)}(r^*) - \hat{u}_r^{(1)}(r_m)] = 0, \tag{F 34}$$

where

$$\mathscr{J} = \int_{r_m}^{r^*} \hat{u}_z^{(1)}\, dr, \tag{F 35}$$

r^* is the explosive charge radius, and $r_m < r^*$ is where the match to our interior explosive solution takes place (approximately one reaction-zone length into the explosive). The velocity $\hat{u}_r^{(1)}(r^*)$ can be obtained from (F 26), and $\hat{u}_r^{(1)}(r_m)$ can be found with the aid of (5.7),

$$\delta\hat{u}_r^{(1)}(r_m) = \frac{(1+t)}{(\gamma+1)\,\delta\mathscr{L}}\{1-[1-(\delta\mathscr{L})^2(\gamma^2-1)]^{\frac{1}{2}}\}, \tag{F 36}$$

which for small $(\delta\mathscr{L})$ is $\quad \delta\hat{u}_r^{(1)}(r_m) = \delta\mathscr{L}\dfrac{(1+t)(\gamma-1)}{2} + \ldots$ (F 37)

Equation (F 34) can now be considered as an ordinary differential equation for $\mathscr{J}(t)$. Solving this equation, and requiring that $\mathscr{J}(1) = 0$ and $\mathscr{J}(0)$ is bounded, forces $\mathscr{L}$ to be

$$\mathscr{L} = 2\gamma + 2\gamma(\gamma-1)\ln[(\gamma-1)/\gamma], \tag{F 38}$$

when the rate of equation (4.5) is used. Therefore, without calculating the details of the rather complex rotational flow that exists in the explosive near the explosive/inert boundary, we can translate information about the confining inert to the interior explosive flow. The value of δ, defined in § 3, is the tangent of the streamline deflection angle at the intersection of the shock and the explosive/inert interface.

I acknowledge many useful and stimulating discussions with W. C. Davis, Ray Engelke, and Wildon Fickett. This work was supported by the U.S. Department of Energy and the Air Force Office of Scientific Research.

REFERENCES

Bdzil, J. B. 1976 In *6th Symp. on Detonation*, ACR-221, pp. 352–370. U.S. GPO.

Campbell, A. W. & Engelke, R. 1976 In *6th Symp. on Detonation*, ACR-221, pp. 642–652. U.S. GPO.

Campbell, A. W. Malin, M. E. & Holland, T. E. 1955 In *2nd ONR Symp. on Detonation*, pp. 336–359. Office of Naval Research.

Comstock, C. 1972 *SIAM Rev.* **14**, 433–446.

Courant, R. & Friedrichs, K. O. 1948 *Supersonic Flow and Shock Waves*, pp. 273–293. Interscience.

DAVIS, W. C. 1964 Los Alamos Scientific Laboratory, unpublished data.

DAVIS, W. C. 1965 Los Alamos Scientific Laboratory, unpublished data.

DAVIS, W. C. 1976 In *6th Symp. on Detonation*, ACR-221, pp. 637–641. U.S. GPO.

DAVIS, W. C., CRAIG, B. G. & RAMSAY, J. B. 1965 *Phys. Fluids* **8**, 2169–2182.

DREMIN, A. N. & SAVROV, S. D. 1966 *Fizika Goreniya i Vzryva* **2**, 36–46.

EYRING, H., POWELL, R. E., DUFFEY, G. H. & PARLIN, R. B. 1949 *Chem. Rev.* **45**, 69.

FICKETT, W. & DAVIS, W. C. 1979 *Detonation*, p. 52. University of California Press.

HAYES, W. D. 1957 *J. Fluid Mech.* **2**, 595–600.

HAYES, W. D. & PROBSTEIN, R. F. 1966 *Hypersonic Flow Theory*, vol. 1, p. 129, p. 21. Academic.

JONES, H. 1947 *Proc. Roy. Soc.* A **189**, 145.

MALIN, M. E. 1955 Los Alamos Scientific Laboratory, unpublished data.

MORSE, P. & FESHBACH, H. 1953 *Methods of Theoretical Physics*, vol. 1, pp. 21–39. McGraw-Hill.

RAO, P. O. 1973 *A.I.A.A. J.* **11**, 1352–1354.

TSUGÉ, S., FURUKAWA, H., MATSUKAWA, M. & MAKAGAWA, T. 1970 *Astronautica Acta* **15**, 377–386.

VAN DYKE, M. 1975 *Perturbation Methods in Fluid Mechanics*, pp. 182–192. Parabolic.

WATSON, R. W. 1970 In *5th Symp. on Detonation*, ACR-184, pp. 169–174. U.S. GPO.

WOOD, W. W. & KIRKWOOD, J. G. 1954 *J. Chem. Phys.* **22**, 1920–1924.

ZELDOVICH, IA. B. & KOMPANEETS, A. S. 1960 *Theory of Detonation*, p. 160. Academic.